



POLITECNICO DI TORINO

Master degree course in Aerospace Engineering

Master Degree Thesis  
in  
Aerospace Engineering

# **Pollutant emissions estimation from subsonic and hypersonic civil aircraft**

Study of emissions in subsonic, supersonic and hypersonic flight, based on  
the Boeing Fuel Flow Method

## **Supervisors**

Prof. Roberta Fusaro  
Prof. Nicole Viola  
Prof. Davide Ferretto

## **Candidates**

Elia MANTELLI  
matricola: s265662

2020 - 2021



*A Lidia ed Aldo*

## **Abstract**

The aim of the thesis is to analyze and compare the emissions of subsonic, supersonic and hypersonic aircraft through the Boeing Fuel Flow Method. In the first part of the work, a relationship was searched between the fundamental quantities of each subsonic engine, Overall Pressure Ratio and By Pass Ratio, and polluting emissions, through the analysis of the ICAO database. A Matlab code was therefore used to read and save the data reported in the Excel database, then interpolating them according to various criteria. Subsequently, starting from the same data, a Matlab code was developed to calculate the Emission Index of each engine through the Fuel Flow Method, and to be able to have an indicative value of emissions during a typical mission. In the last section concerning subsonic flight, FFM was implemented even in the case of liquid hydrogen, rather than kerosene. In the supersonic field, after a brief introduction on the different architectures of supersonic engines, an analysis of the data of the Stratofly hypersonic engine (Dual Mode Ramjet) was carried out. Finally, a possible adaptation of the Fuel Flow Method to the supersonic and hypersonic flight, and an example of calculation using the Stratofly scramjet data, are proposed.



# Contents

<b>1</b>	<b>Aviation and Environment</b>	<b>5</b>
1.1	Actual situation . . . . .	5
1.2	Local Air Quality: LAQ . . . . .	7
1.3	Polluting emissions: Status and Reduction . . . . .	9
1.3.1	$CO$ . . . . .	10
1.3.2	$CO_2$ . . . . .	10
1.3.3	$NO_x$ . . . . .	11
1.3.4	$H_2O$ . . . . .	11
1.4	Noise . . . . .	13
1.5	Sustainable Aviation Fuel and hydrogen fuel . . . . .	15
1.5.1	Infrastructure requirements for hydrogen fuel . . . . .	17
<b>2</b>	<b>Subsonic flight</b>	<b>21</b>
2.1	Subsonic engine architectures . . . . .	21
2.1.1	Turboprop . . . . .	22
2.1.2	Turboshaft . . . . .	23
2.1.3	Turbojet . . . . .	24
2.1.4	Turbofan . . . . .	25
2.2	Decreasing consumption . . . . .	27
2.2.1	Changes to improve performance to classic architecture . . . . .	28
2.3	Innovative technologies and architectures . . . . .	31
<b>3</b>	<b>Data analysis for subsonic flight</b>	<b>35</b>
3.1	Fourth degree polynomial . . . . .	35
3.1.1	Turbofan separated flow . . . . .	36
3.1.2	Turbofan with mixer . . . . .	39
3.2	Curve fitting . . . . .	41
3.2.1	Turbofan separated flow . . . . .	43
3.2.2	Turbofan with mixer . . . . .	45
3.3	Final results . . . . .	47
<b>4</b>	<b>Subsonic Emission Method during LTO and CCD</b>	<b>49</b>
4.1	Calculation of the quantity of emissions . . . . .	49
4.2	Fuel Flow Method 2 . . . . .	51
4.2.1	Methodology . . . . .	56

4.2.2	Matlab Code . . . . .	57
4.3	Fuel Flow Method for $LH_2$ combustion . . . . .	59
<b>5</b>	<b>Hypersonic flight</b>	<b>63</b>
5.1	Ramjet . . . . .	64
5.2	Scramjet . . . . .	66
5.3	Air Turbo Ramjet (ATR) . . . . .	68
5.3.1	LACE . . . . .	70
5.3.2	SABRE . . . . .	71
<b>6</b>	<b>Supersonic emission method</b>	<b>73</b>
6.1	Modifications to the subsonic method . . . . .	73
<b>7</b>	<b>Application of supersonic emission method</b>	<b>77</b>
7.1	Emissions during supersonic mission . . . . .	81
7.2	Comparison between Stratofly and A380 . . . . .	82
<b>8</b>	<b>Conclusions</b>	<b>87</b>
	<b>Bibliography</b>	<b>89</b>

# Chapter 1

## Aviation and Environment

### 1.1 Actual situation

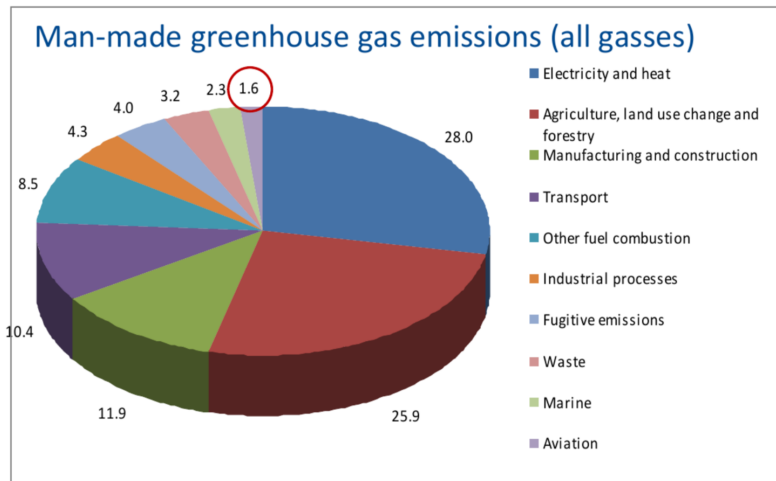
The growth of air traffic is having an increasing environmental impact. Concerns about climate change are also increasing, and aviation is expected to contain the growth of its carbon footprint in the context of the global efforts to reduce  $CO_2$  emissions.

The aviation sector accounts for approximately 2% of global anthropogenic  $CO_2$  emissions, including international and domestic aviation. Reactions to aircraft noise still exist around many world airports, and there is growing concern about local air quality ( $LAQ$ ) with an increased emphasis on small particles from engine combustion, referred as non-volatile Particulate Matter ( $nvPM$ ). [7] In fact in the last few years, the International Civil Aviation Organization, in addition to the evolution of technological developments, is monitoring the evolution of scientific knowledge related to the impacts of aviation on the global climate.



Figure 1.1. Global air traffic

Aviation affects global climate through both  $CO_2$  and  $non - CO_2$ . Other  $non - CO_2$  factors such as ozone, methane or water vapor also affect global warming. While  $CO_2$  impacts on the climate are well understood, there are important uncertainties regarding



some of the *non* –  $CO_2$  impacts and the underlying physical processes. That is why, since 1997, ICAO has requested scientific institutions to further investigate these effects in order to develop appropriate measures.[7]

This resulted in the publication of the “IPCC Aviation and the Global Atmosphere report” in 1999, which provided the scientific basis for impacts of aviation on global climate and highlighted the state of understanding, the aviation technology and the socio-economic issues associated with aviation. Twenty years after the publication of this report, these estimates of aviation climate changing could be enhanced by a new international scientific assessment. In the absence of such report, in order to update and strengthen the scientific base, the information contained in the IPCC 1999 report is being supplemented by the work carried out by ICAO and the Committee for Aviation Environmental Protection (CAEP).

For climate change, the primary concerns are emissions of  $CO_2$ ,  $NO_x$  and *nvPM*. Also of concern are persistent contrails which lead to cirrus clouds when the atmosphere is ice-super-saturated. A significant complication arises because the emissions (or their subsequent transformations) have different residence times in the atmosphere.

$CO_2$  is of particular concern because of its exceptionally long residence time (thousands of years). Although *nvPM* is implicated in cloud formation, the processes are less well understood. Contrails, leading to cirrus clouds and aircraft induced cloudiness, have large environmental impacts but have short life (hours). There is high confidence in the estimation of global warming due to  $CO_2$  whereas for all other emissions there is a significant level of uncertainty which has to be reduced.

Optimization of air traffic management and operational procedures is a key element to avoid greenhouse gas emissions from aviation. The Global Air Navigation Plan (*GANP*) and the Aviation System Block Upgrades (*ASBUs*) are major initiatives developed by ICAO to that end. The *GANP* is a strategy to achieve a global interoperable air navigation system, that is directed to all users during all phases of flight. It meets agreed levels

of safety, provides for optimum economic operations, is environmentally sustainable and meets national security requirements. The *ASBUs* provide a roadmap to assist air navigation service providers in the development of their individual strategic plans and investment decisions.

Also Sustainable Aviation Fuels (*SAF*) have an important role in reducing  $CO_2$  emissions from aviation. They are an important element of ICAO’s measures to mitigate climate change. [7]

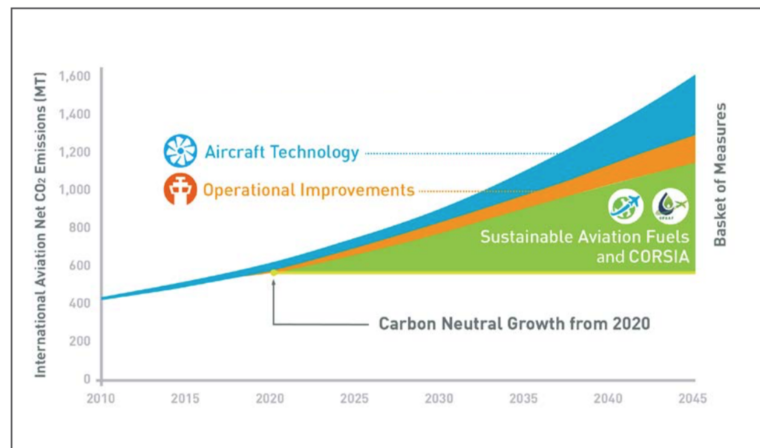


Figure 1.2. Contribution of measures for reducing international aviation net  $CO_2$  emissions

## 1.2 Local Air Quality: LAQ

One of ICAO’s environmental goals is to limit or reduce the impact of aviation emissions on local air quality (*LAQ*). Starting the late 1970s, ICAO has been performing measurements of emissions generated by aircraft engines in the proximity of the airport and by relevant airport sources. The Volume II of Annex 16 to the Convention on International Civil Aviation contains Standards for aircraft engine emissions and is accompanied by the related guidance material and technical documentation. Following the latest successful adoption of the *CAEP/10* *nvPM* Standard based on visibility criterion, *CAEP/11* agreed on *nvPM* mass and number Standard, moving it towards consideration for adoption by the ICAO Council in the next year. ICAO provisions on *LAQ* also address liquid fuel venting, smoke (which is expected to be superseded by the *nvPM* Standard), and the main gaseous exhaust emissions from jet engines, namely: hydrocarbons (*HC*), oxides of nitrogen (*NO<sub>x</sub>*), carbon monoxide (*CO*). [7]

The engine certification process is based on the Landing and Take-off (*LTO*) cycle. This *LTO* cycle representing pollutant emissions in the proximity of airports consists of four operating modes, which involve a thrust setting and a time-in-mode shown in 1.3 on the following page.

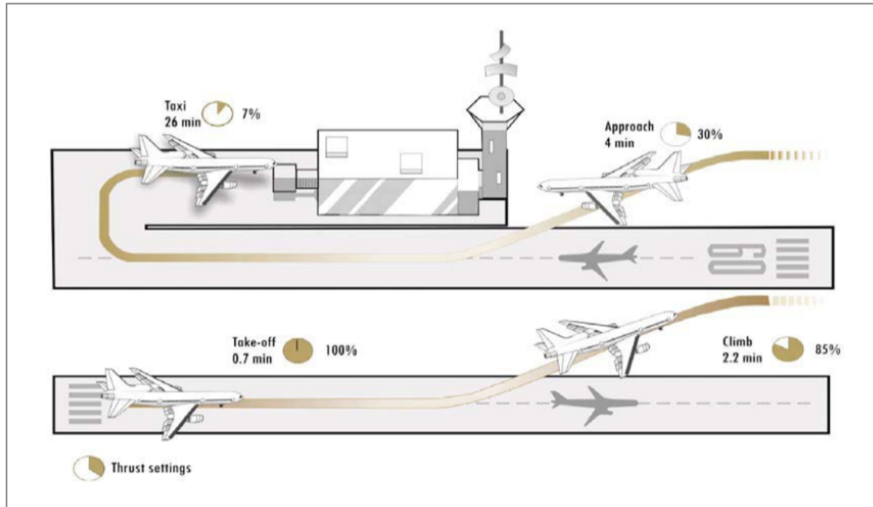


Figure 1.3. Time in operating mode and thrust setting

The effects of atmospheric pollutants are exerted on humans, animals, plants and more generally on the environment. The effects on humans are evaluated by epidemiological studies (which correlate increases in mortality with excursions in pollutant concentration), studies on animals (which can be subjected to high doses, but whose response may not be the same of man), as well as cell cultures in vitro (i.e. detached from the organism to which they originally belonged) and in vivo (on the organism in life). In some cases the presence of a threshold is found (i.e. the pollutant is not harmful below a certain concentration), while in others there is still an effect, although the concentration is low. Often, the threshold existence is difficult to ascertain. Aircraft emissions of pollutants are estimated to be responsible for about 8000 premature deaths per year, which represent about 1 % of premature deaths due to alterations in air quality by all types of air sources emissions. This number should be compared with the estimated 470,000 premature deaths per year due to ozone at ground level, and about 2,100,000 premature deaths per year due to particulate matter. Estimates the effect of global warming (to which aviation also makes a contribution) range from 300,000 to 5,000,000 premature deaths per year. These numbers underline that, while it is certainly necessary to reduce aviation emissions, this will still be ineffective if not accompanied by similar measures in all fields of human activities. [7]

Phase	Time [min]	Thrust
Take-off	0.7	100% $F$
Climb	2.2	85% $F$
Approach	4.0	30% $F$
Taxi/ground idle	26.0	7% $F$

Table 1.1. Time in operating mode and thrust setting

### 1.3 Polluting emissions: Status and Reduction

Emissions from aviation fuel combustion affect human health and welfare through air quality degradation as well as through climate change. Under all reasonable scenarios of technology change and aviation growth, total fleet fuel burn and the mass of  $NO_x$  emissions are expected to continue to rise. Aircraft emit emissions that change air quality, either on or near the ground and during cruise. At cruise altitudes, the emissions undergo chemical and physical transformations. The climate impact of  $NO_x$  emissions is still thought to be

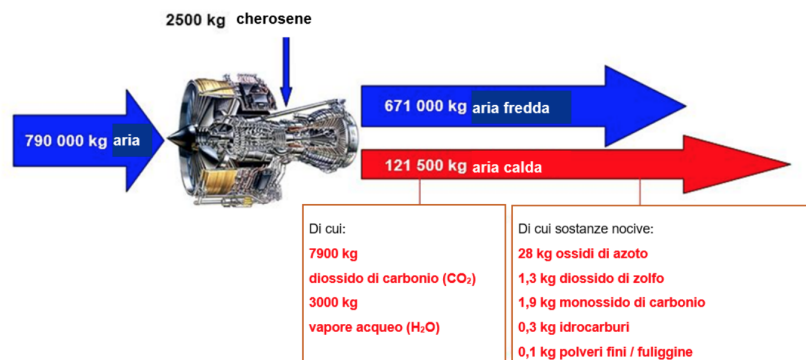


Figure 1.4. Use of a typical motor for one hour

significant relative to  $CO_2$ , though less than in previous reviews. Some studies note that aircraft emissions emitted at cruise altitudes may potentially reduce surface air quality and affect human health. Historically, the focus has been on the landing and take-off (*LTO*) cycle, when aircraft are at their closest to populations around airports, because concentrations fall down rapidly with increasing distance from the airport.

Nitrogen dioxide ( $NO_2$ ) from  $NO_x$  emissions and its photochemical derivative, ozone ( $O_3$ ), are identified as harmful to human health, though quantification of this is unreliable. More recently, attention has been directed at non-volatile particulate matter (*nvPM*), and of particular concern are ultrafine particles, less than 100 nano-metres, which is the particle size produced by aircraft combustors. Previously ‘smoke’ was a major concern, and standards were based on opacity measurements. In addition,  $NO_x$  and oxides of sulfur ( $SO_x$ ) are precursors of secondary volatile *PM* formation, which takes place over considerable distances away from the source. The contributions to local concentrations of pollutants from *LTO* operations are higher than the contributions from cruise, but the numbers of people affected are relatively small. For emissions from higher altitudes, the increase in concentration at the surface is much smaller than for *LTO* but much larger numbers of people are potentially affected. [9]

A brief description of the main pollutants with their characteristics is reported in the following sections:

### 1.3.1 CO

Carbon monoxide has a very strong affinity for blood hemoglobin, 220 times stronger than oxygen, causing the formation of carboxyhemoglobin. When the concentration of CO exceeds the very low background atmospheric values (i.e. measured far from sources of pollution), as can happen indoors, in the city (due to vehicular traffic), or in the proximity of airports, it leads to non-negligible concentrations of carboxyhemoglobin (unable to carry oxygen) in the blood. It can be lethal for prolonged exposure (8 hours), already for concentrations of carbon monoxide in the air  $XCO = 0.02\%$ . [5]

The background concentration of CO is higher in the northern hemisphere, around 120 ppb, where there are most of the emissions. In the southern hemisphere, lower values are recorded (50 - 60 ppb). Since the average life relatively short; around 0.2 years, this amount is largely destroyed by natural processes before its concentration can become uniform throughout the earth's atmosphere. The concentration in cities, near airports and in closed environments can be much higher and therefore be dangerous.

### 1.3.2 CO<sub>2</sub>

The contaminants CO<sub>2</sub>, CH<sub>4</sub>, N<sub>2</sub>O and others contribute to the greenhouse effect, while the nitrogen oxides NO<sub>x</sub> and also the N<sub>2</sub>O contribute to the depletion of the stratospheric ozone layer.

Nowadays, CO<sub>2</sub> emissions are the most understood and the most popular way to measure the aviation impact on climate. Aircraft combustion engines emit 3.15 kilograms of CO<sub>2</sub> for every kilogram of kerosene burned in flight. This CO<sub>2</sub> remains in the upper atmosphere for 50 to 100 years. [10]

To calculate the emissions of CO<sub>2</sub> the following formula is used:

$$CO_2 = \frac{(1/SAR)_{AVG}}{(RFG)^{0.24}}$$

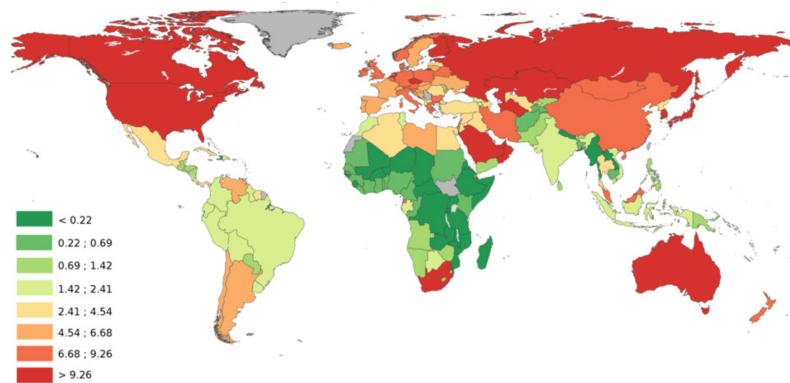
The  $1/SAR$  value is established according to the 3 possible masses of the aircraft:

- high gross mass:  $92\%MTOM$
- simple arithmetich average of high gross mass and low gross
- low gross mass:  $(0.45MTOM) + (0.63MTOM)^{0.924}$

The following symbols appear in this formula:  $SAR$  is the specific air range ( $km/kg$ ),  $AVG$  is the average, and  $RFG$  is the reference geometric factor.

The CO<sub>2</sub> emissions should not exceed the defined value. For airplanes with a maximum take-off mass less than or equal to 60 000kg, maximum permitted value is  $10^{-2.7378+(0.68131\log(MTOM))+(-0.0277861(\log(MTOM))^2)}$ . For the airplane with a maximum take-off mass greater than 60 000 kg, and less than or equal to 70 395 kg, maximum permitted value is 0.764. [10]

The maximum permitted value for airplanes with take-off mass greater than 70 395 kg is  $10^{-1.412742+(-0.020517\log(MTOM))+0.0593831(\log(MTOM))^2}$

Figure 1.5. Emissions of  $CO_2$  pro capite

### 1.3.3 $NO_x$

Nitrogen oxides are the other (in addition to  $SO_x$ ) main contributor to acid rain (contributing for about 25 - 30 % of the total, as nitrogen dioxide  $NO_2$ , in contact with humidity air, generates nitric acid). They are respiratory irritants (in particular nitrogen dioxide  $NO_2$  is already detected in a concentration of about 1 ppb in unpolluted air), and promote, in the presence of hydrocarbons in the air, the formation at ground level of ozone and secondary particles. They also promote the depletion of the stratospheric ozone layer (but it must be said that CFCs - chlorofluorocarbons are much more harmful), and nitrous oxide  $N_2O$  is also a powerful greenhouse gas. [5]

### 1.3.4 $H_2O$

The effect of clouds on heating is twofold: on the one hand they reflect the incident sunlight during the day, thus decreasing the fraction that reaches the ground, on the other hand they retain part of the outgoing infrared radiation at night. For low-altitude clouds, the first effect prevails over the second, thus leading to cooling.

As for the *contrails*, it was recently ascertained (based on the climatic trends recorded in the United States in the days immediately following the attacks of 11 September 2001, when the airspace was closed for several days) that the the resulting balance determines a positive contribution to the growth of the earth's temperature, thus contributing to the greenhouse effect. In particular, it was verified that in those days the diurnal temperature excursion (difference between the maximum and minimum daily temperatures) was about 1.1 ° C wider than normal (precisely because the absence of contrails determined higher maximum temperatures during the day, and lower minimum temperatures at night). To understand the effect of this increased excursion on global warming, it is necessary to consider that the power of the radiation emitted per unit of surface from the Earth (therefore outgoing) is proportional to  $\sigma T^4$ , where  $\sigma = 5.67 \cdot 10^{-8} \frac{W}{(m^2 K^4)}$  is the Stefan-Boltzmann constant, and  $T$  the value of the local terrestrial (absolute) temperature. Due to the non-linearity of this relationship, the positive temperature peaks determine an increase in the

radiative flux outgoing from the Earth  $\Delta(\sigma T^4)+$  in an absolute value greater than the reduction  $\Delta(\sigma T^4)-$  which occurs in correspondence to negative peaks, with the consequence that the net flow out of the Earth is greater as the diurnal temperature excursion increases. The presence of contrails, reducing the diurnal temperature range, therefore reduces the heat flow out of the Earth, thus aggravating global warming. [5]

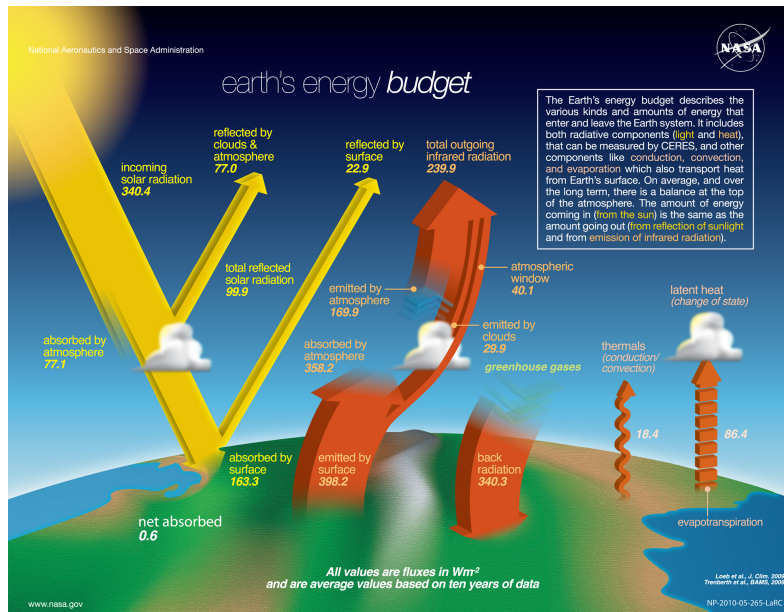


Figure 1.6. Global warming

It has been estimated that the contribution of contrails to global warming is approximately 1.1 % of the total, which must be added to the contribution of 2 % of carbon dioxide emissions from aircraft engines. This could lead to an increase in terrestrial temperature of an entity estimated between 0.01 and 0.1 degrees Celsius per decade (this wide field of uncertainty is indicative of the still incomplete understanding of the phenomenon).

To limit the contrails and their negative effects, the aircraft's cruise flight altitude could be adjusted. In particular, it has been found that it would be necessary to increase it at medium latitudes (in order to fly in drier air), and instead reduce it near the tropics (in order to fly where the air is warmer), but both these options pose problems. Flying at higher altitudes means flying where the ozone concentration is higher, resulting in a greater effect of  $NO_x$  emissions from engines. Flying at lower altitudes would lead to greater crowding of low-altitude airways, with consequent traffic control problems. A much less penalizing approach would be to reduce the flight altitude only when weather conditions favorable to the persistence of the contrails occur, or to avoid crossing areas where conditions favorable to persistence exist. However, this presupposes a real-time monitoring of weather conditions, and a consequent redefinition of the airways as a function of them, still posing significant problems to air traffic management. We could then, in

theory, concentrate the flights in the periods of the day less favorable to the formation of contrails (sunrise / sunset), but this obviously would limit in an unacceptable way the productivity of an airplane, as well as being inapplicable for long routes. It has also been thought to break up the ice crystals of the contrails by means of microwave or ultrasound, but these studies are still in its infancy.[1]

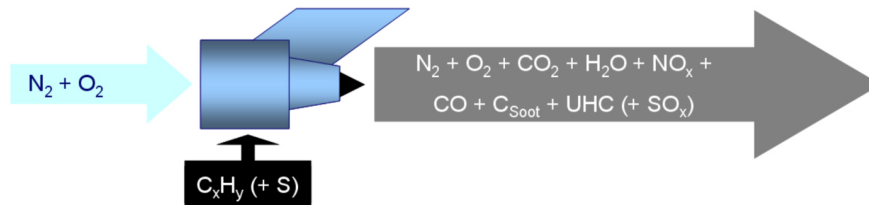


Figure 1.7. Hydrocarbon combustion

## 1.4 Noise

Noise is another very important form of pollution. In fact a further problem near airports is due to noise pollution.

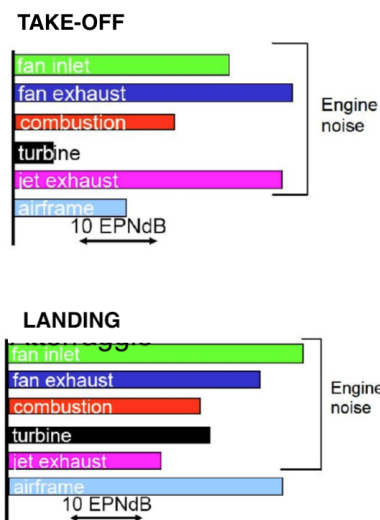


Figure 1.8. Noise during LTO cycle

In 1968, the 16th ICAO Assembly instructed the ICAO Council to establish international specifications and associated guidance material relating to aircraft noise; and to include, in appropriate existing Annexes and other relevant ICAO documents, and possibly in a separate Annex on aircraft noise (*Annex 16, Vol. I*), such material as the description and methods of measurement of aircraft noise and suitable limitations on the noise caused by aircraft that was of concern to communities in the vicinity of airports.[8]

There has been a large increase in studies in recent years examining associations of noise exposure with health outcomes. The best epidemiological evidence relates to cardiovascular disease, which includes analyses from population-based studies covering millions of individuals, in particular for new cases of ischaemic heart disease.

Findings for aircraft noise are consistent with those for road traffic noise. Results from epidemiological studies are also supported by evidence from human and animal field and laboratory

experimental studies showing biological effects of noise on mechanistic pathways relating to risk factors for cardiovascular disease.

This experimental evidence, together with consistency with findings for road traffic noise, supports the likelihood of a correlation between aircraft noise with heart diseases observed in epidemiological studies. However, the exact magnitude of the exposure-response estimate for heart disease varies between studies and best estimates (obtained by combining results from good quality studies in a systematic review) are likely to change as further studies add to the basic evidence.

An aircraft can employ noise reduction systems that change its configuration or operating condition to reduce noise, or implement devices or subsystems that directly reduce or counteract sound emissions. Two categories, variable noise reduction systems (VNRS) and selectable noise reduction systems (SNRS), have been defined to address differences in activation/actuation for these systems.

A VNRS is an integral design feature, or subsystem, of an aircraft that automatically changes the configuration or operating condition of the aircraft to reduce noise.

In order to estimate noise exposure at airports, a decibel measurement called Day-Night Noise Level (DNL) was adopted. It is an index that estimates the ordinary daily noise (morning and night, day and night) created by continuous exposure to a series of events that occur over a period of time equal to one year. The standards for aircraft noise, on the other hand, were established based on a measure of the noise actually perceived by human hearing at that moment; in fact, since the perception of the human ear is not exactly proportional to the decibel scale, some psycho-physiological aspects must also be taken into account when measuring the phenomenon. The most used scale for acoustic measurements is that of the perceived noise level (PNL). Another metric often used is the one that refers to the actually perceived noise (EPNL, Effective Perceived Noise Level) detected in EPNdB which improves the results provided by an evaluation through the NLP as it also takes into account the duration and the presence of low frequency tones in the phenomenon that is being analyzed. [8]

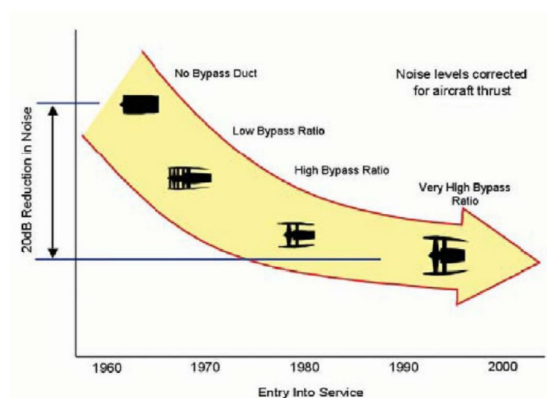


Figure 1.9. Progressive reduction of noise in the various families of engines

## 1.5 Sustainable Aviation Fuel and hydrogen fuel

Sustainable aviation fuels (SAF) are one element of the ICAO basket of measures to reduce aviation emissions, which also includes technology and standards, operational improvements, and the Carbon Offsetting and Reduction Scheme for International Aviation (CORSIA).

Sustainable Aviation Fuels can play a major role in reducing international aviation emissions.

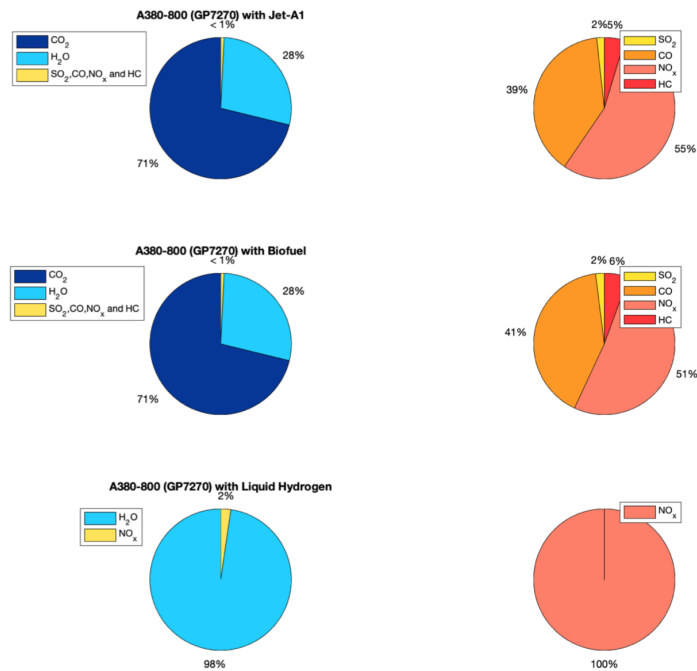
Since the first flight on SAF in 2008, considerable progress has occurred in all aspects of production, certification and deployment. Today SAF are being produced and used in commercial flights every day. While the current volumes being produced are low (<1% of total jet fuel demand), these volumes can be substantially increased with coordinated support including effective policy frameworks. To date, about 40 million liters of SAF have been produced and each of the five technical pathways to produce SAF have been used for commercial flights. These technical SAF pathways to produce SAF typically deliver a 60-80% reduction in  $CO_2$ , which is equivalent to 25,000 cars being taken off the road since regular use began in 2016.

Despite this good news, it must be noted that the 10 million liters of SAF per annum represents just 0.01% of total fuel uptake. Clearly, the production of SAF needs to increase dramatically to make a more substantive environmental impact. Over the past 18 months there has been considerable commercial SAF activity with the announcement from airlines of new forward purchase agreements and new commercial construction activity which has included both new SAF plants as well as the expansion of existing facilities.

Looking out to 2025, publicly announced projects alone could push SAF uptake in aviation to 3.5 billion liters annually. It is not unreasonable to assume that as-yet-unannounced projects will double that number, representing nearly 2% of total fuel demand by 2025. Further increases in SAF production and uptake will be aided by the technical approval of new fuel pathways, investment in production capacity, and innovative collaborations.

Further increases in SAF production and uptake will be aided by the technical approval of new fuel pathways, investment in production capacity, and innovative collaborations.

An alternative, capable of almost totally canceling the impact of aviation on global warming, and greatly reducing the impact on the stratospheric ozone layer, is to adopt



hydrogen as fuel instead of kerosene. Since there is no carbon in the fuel, carbon dioxide emissions would be totally eliminated. However, the use of hydrogen poses several problems. The hydrogen low density leads to a somewhat lower energy release per unit of volume, thus requiring more tanks bulky, for releasing energy per unit of mass equal to about 2.8 times that of kerosene. Assuming that hydrogen is stored on board in liquid form, therefore in the cryogenic state (which means, at atmospheric pressure, at temperatures of no more than 20 K, or -253 °C), its density would be just  $71 \text{ kg/m}^3$  (compared to about  $800 \text{ kg/m}^3$  for kerosene), so the energy density per unit of volume is 3.9 times lower than that of kerosene. This therefore requires very bulky tanks (therefore heavy, which cause an increase in the wet surface of the aircraft, resulting in greater aerodynamic drag); the problem is accentuated by the need to provide thermal insulation around the tanks (and also to the fuel lines). The tanks can then be subjected to an stress due to the fact that it is desirable to keep the pressure inside the tanks at an approximately atmospheric value, instead of letting it drop to the ambient value at high altitude (because the boiling temperature of liquid hydrogen drops further as pressure decreases). The tank walls must therefore resist the difference between internal and external pressure, which implies the need to adopt thicker, therefore heavier, walls. These bulky tanks could be placed at the top of the fuselage. [3]

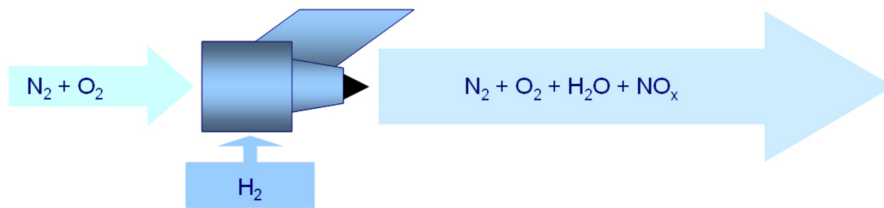


Figure 1.10.  $LH_2$  combustion

A hydrogen-powered plane, while not emitting  $CO_2$ , would lead to higher emissions of  $H_2O$  (in the form of gas). The lack of condensation nuclei due to the absence of soot would, however, allow to contain the formation of contrails, and in particular the condensation around these nuclei of the moisture naturally present in the atmosphere. The only residual emissions would be those of  $NO_x$ , which however could be strongly contained by adopting premixed combustion. The lower flammability limit of a hydrogen-air mixture corresponds in fact to an equivalence ratio of just 0.1 (the lower flammability limit of a kerosene/air mixture is much higher). By adopting a very lean premixed combustion in the primary area of the chamber, it is possible to contain the flame temperature, with consequent relief of thermal  $NO_x$  emissions, highly sensitive to temperature, albeit with a certain performance penalty, in particular the specific thrust. [4] However, it should be noted that hydrogen is not an energy source itself (there are no hydrogen deposits), but simply an energy vector. Over 90% of global hydrogen production derives from the methane reforming process, in which the carbon atom contained in methane is oxidized to  $CO_2$  (which is therefore not released at altitude, but in the production process, with the same effect on global warming). It will therefore be necessary to produce hydrogen

through electrolysis of water (which produces only hydrogen and oxygen), using electricity produced from renewable sources (ie not from the combustion of fossil fuels). It should also be noted that the production of liquid hydrogen is about 170  $t/d$  in the USA, 19  $t/d$  in Europe, while only for intra-European flights it would be necessary, assuming that the entire air fleet was converted hydrogen, 30,000  $t/d$ . It is therefore necessary to provide for adequate infrastructures, which include in particular plants for the production of hydrogen by electrolysis near airports. [3]

### 1.5.1 Infrastructure requirements for hydrogen fuel

Sustainable and environmentally friendly production processes including photolysis, electrolysis and biomass gasification are being developed and will produce ‘green hydrogen’ within the coming decades. Furthermore Munich Airport has built and proven, on a small-scale, that a hydrogen based infrastructure at an airport can run efficiently and affordably. Combined with innovative and currently working solutions for the transport of hydrogen, during the period from 2025 to 2040, a smooth transition to liquid hydrogen compatible airports and aircraft is expected. Twenty to thirty years will be needed to build prototype aircraft that can fully test a liquid hydrogen fuel and powerplant system. Overall there are two main requirements for a successful implementation of this concept: the aircraft and airport must work on liquid hydrogen and the total cost must not be any higher than flying with kerosene. [2]

Beyond the implications for aircraft design discussed in the next chapters, switching to  $LH_2$  would have major implications for the fuel supply chain, airport infrastructure and operations, and the air travel system as a whole.

In order to analyze the required infrastructure, we consider two scenarios for aircraft deployment.

In the *efficient decarbonization scenario*; hydrogen plays a role where it is the most cost efficient means of decarbonization. In this scenario, aircraft up to medium-range will start to be replaced with hydrogen aircraft by 2030-2040, representing the earliest potential entry into service dates of aircraft in each segment. After a ramp up of manufacturing capacity over three to four years, all new aircraft in commuter and short-range and 50% of medium-range aircraft would be powered by hydrogen. In this scenario, 40 percent of all aircraft are switched to  $LH_2$  by 2050, while the remainder would be powered by other sustainable aviation fuels like synfuel and/or biofuels. [2]

In a *maximum decarbonization scenario*; hydrogen aircraft would start to replace all aircraft for ranges of up to 10,000 kilometers after 2028-2038, representing the first conceivable entry-into-service dates with ambitious assumptions. After a ramp-up of manufacturing capacity over three to four years, all new aircraft up to a 10,000 km range would be powered by hydrogen. In this scenario, 60 percent of all aircraft are switched to  $LH_2$  by 2050, and the rest would be powered by synfuel and/or biofuels.

In these two scenarios, the global demand for hydrogen would reach approximately 10 or 40 million tons of  $LH_2$  by 2040 per annum, and approximately 40 or 130 million tons by 2050. [1]

In the early years, given the amount of refueling required and the primary focus on

regional airports – which already often use refueling trucks – a major overhaul of the refueling infrastructure at airports is not likely to be needed. The number of refueling trucks required is roughly double the number needed for kerosene or synfuel but comprises only a small share of the total existing refueling fleet in this time frame, so the implications on ground traffic would be limited. These  $LH_2$  refueling trucks are very different to existing refueling trucks and would require a different training and a safety assurance framework for operations, but these are manageable challenges to overcome. In addition, refueling times would likely stay within the required turnaround times of shorter-range aircraft.  $LH_2$  hoses could attain the same flow rate in the short-term as kerosene/synfuel hoses – about 900 liters per minute – if the right investments are made to accommodate the hoses' heavier weight and lower maneuverability. Given  $LH_2$ 's lower volumetric density,  $LH_2$  refueling would still be much slower, but if the amount of hoses were doubled from one to two, the refueling of a sample short-range airplane would take from 20 to 30 minutes, which would still be within turnaround times. The major remaining question concerns safety and taking the necessary precautions when refueling, which could potentially compromise the ability to conduct parallel operations during the turnaround.

If  $LH_2$  is trucked in from outside, liquefaction would not have to take place at the airport. The needed three-day storage of  $LH_2$  (around 90 tons for regional airports) would require only limited space (about 100 square meters). The size of the required safety perimeter around this storage space – as mandated by the SEVESO Directive in the EU, which regulates hazardous chemicals – is not yet known, but the re-



Figure 1.11. Production, distribution and use of liquid hydrogen

gional airports that would likely be early movers tend to have more space and might accommodate this additional infrastructure more easily. Finally, in early years when not all airports have an  $LH_2$  infrastructure, it is worth noting that flights that are diverted may get stuck at an airfield waiting for  $LH_2$  resupply by truck if that airfield is not cleared for  $LH_2$  refueling. Diversions are common across the industry, so this would be an early stage-challenge. While these challenges exist, all in all, the technical feasibility of establishing  $LH_2$  infrastructure in the early years (up to 2040 in the efficient decarbonization scenario and 2035 in the maximum decarbonization scenario) is strong, even within the constraints of the current infrastructure. The major challenge will likely be in ensuring the required coordination between fuel providers, airports, aircraft manufacturers, and airlines as they develop the new industry in tandem.

While supply-side challenges will be significant in 2050, they will not be unique in a future energy system that partially relies on hydrogen. The challenges affecting the airport refueling infrastructure and operations are unique, however, and will require significant development and planning to overcome. They include searching for scalable refueling technology, optimizing refueling practices, and reconfiguring airport infrastructure to introduce parallel fuel systems.

The first challenge to develop scalable refueling technologies. In many large airports today, hydrant pipelines are used to refuel aircraft. These pipelines could be easily adapted to synfuel. To the contrary, by 2040 cryogenic hydrant refueling systems for  $LH_2$  seem to be cost-technically infeasible, as their cost may be as much as five times the cost of conventional hydrant systems. Given this fact, the most viable near-term  $LH_2$  refueling technology seems to be the  $LH_2$  refueling truck. These trucks work well at smaller airports, where kerosene refueling trucks are used today, but at larger airports they could greatly increase ground traffic and pose logistical challenges.



Figure 1.12. Liquid hydrogen tank

shorter-range aircraft segments, refueling times for long-range aircraft may extend beyond their current standard turnaround times. For instance, if a long-range plane has a tank that is 75 percent empty, refueling the tank with kerosene/synfuel using two hoses may take up to 65 minutes, assuming a flow rate of 900 liters per minute per hose. Assuming the same flow rates for  $LH_2$ , even with twice as many hoses, refueling would take 140 minutes. The standard turnaround time for a large jumbo jet is about 120 minutes today. Further research and development will be important to develop economic solutions to push refueling flow rates above 1,000 liters per minute per hose. For large aircraft refueling, automated tank solutions that can handle higher weights of hoses for higher refueling rates may even allow for flow rates at multiples of kerosene today. [2]

For now, the optimal solution is unclear. Larger mobile refueling platforms or even refueling station lots away from boarding gates may be an option. The latter may sound cost-technically infeasible given today's required turnaround times but considering the lengthier refueling times needed for medium- and long-range  $LH_2$  aircraft, an economic case could be made for refueling station lots if they greatly optimize refueling times. In the longer term,  $LH_2$  hydrant pipeline systems may become a viable solution. Refueling practices and operations will also need to be reviewed. Unlike

Beyond longer refueling times, it is unclear whether all or some of the usual turnaround operations could happen in parallel. First, doubling the amount of hoses will cause additional spatial constraints around the aircraft and leave less room for other operations to take place. In addition, it is not certain which turnaround operations would be permitted from a regulatory and safety perspective. Experts agree that new regulations will need to be developed to ensure adequate and safe handling of low temperature  $LH_2$  and its unique properties (for instance, the possible spontaneous ignition on contact with water, asphyxiation risk, and vertical dispersion). The impact on aspects such as ignition free zones around refueling trucks is as yet unclear. For example, some experts suggest that the periphery required around refueling trucks may even be smaller, as  $LH_2$  would not form a pool on the ground but rather evaporate upwards in the air. This shows that safety considerations are still highly preliminary and need to be refined through further research and on-the-ground testing.

The final challenge is to find the capacity to set up two parallel refueling systems at busy, spatially constrained hubs. Spatial requirements are likely to be moderate; for example, if hydrogen production happens off-site, large airports using 500 tons of  $LH_2$  would need less than 25,000 square meters for liquefaction and storage equipment, or about 0.2 percent of Heathrow's footprint today. However, additional capacity may be needed if refueling lots must be installed away from gates and/or gate space is locked for longer periods due to longer refueling times. Finally, airport box sizes may not always be able to accommodate the additional 10 to 15 meters in length needed for the suggested  $LH_2$  medium-range and long-range aircraft designs, which could potentially lead to the need for sizable infrastructure investments. Alternatively, this could lead to constraints on aircraft gate assignments, which would further increase turnaround times and reduce overall infrastructure flexibility. [2]

# Chapter 2

## Subsonic flight

A subsonic aircraft is an aircraft with a maximum speed that is less than the speed of sound (Mach=1). The term technically describes an aircraft that flies below its critical Mach number, typically around Mach 0.8. All current civil aircrafts, including airliners, helicopters and airships, as well as many military types, are subsonic.

Subsonic flight is aerodynamically characterised by incompressible flow, where dynamic pressure changes due to motion through the air cause the air to flow away from areas of high dynamic pressure to areas of lower dynamic pressure, leaving the static pressure and density of the surrounding air constant. At high subsonic speeds, compressibility effects begin to appear.

The propeller is one of the most efficient sources of thrust available and is common on subsonic airplanes and airships. Sometimes it is enclosed in the form of a ducted fan. At higher subsonic speeds and at high altitudes, such as those attained by most airliners, the high-bypass turbofan becomes necessary.

### 2.1 Subsonic engine architectures

The main engine architectures for subsonic flights are the following:

- Turboprop
- Turboshaft
- Turbofan (separated flow or with mixer)
- Turbojet

In the following paragraphs will be described the different types of engines, but the whole chapter will be only focused on turbofans, as they are the most used in civil transport.

### 2.1.1 Turboprop

A turboprop engine is a turbine engine that drives an aircraft propeller.

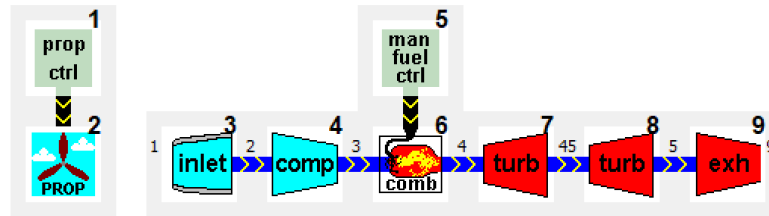


Figure 2.1. Turboprop in GSP

In its simplest form a turboprop consists of an intake, a compressor, a combustor, a turbine, and a propelling nozzle. Air is drawn into the intake and compressed by the compressor. Fuel is then added to the compressed air in the combustor, where the fuel-air mixture then combusts. The hot combustion gases expand through the turbine. Some of the power generated by the turbine is used to drive the compressor. Thrust is obtained by the combusting gases, pushing toward a (vectored) surface in front of the expanding gas.

The remaining power is transmitted through the reduction gearing to the propeller. Further expansion of the gases occurs in the propelling nozzle, where the gases exhaust to atmospheric pressure. The propelling nozzle provides a relatively small portion of the thrust generated by a turboprop.

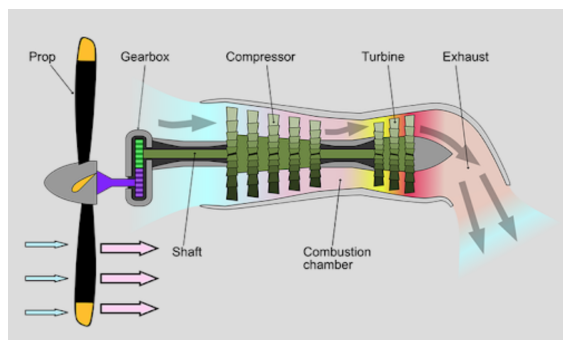


Figure 2.2. Turboprop

In contrast to a turbojet, the engine's exhaust gases do not generally contain enough energy to create significant thrust, since almost all of the engine's power is used to drive the propeller.

The thrust generated by the propeller is generally very small and hence not suitable for flights with high payloads. For this reason it is not considered in this thesis work that deals with international flights or flights with a large number of passengers, in order to have a comparison with the European Stratofly project.

Compared to the turbojet, the turboprop engine allows generally lower cruising speeds and a higher noise level than the turbofan engines, but has lower fuel consumption, greater thrust during take-off and greater efficiency at low altitudes. The possibility of reversing the pitch of the propeller also makes it possible to land in much smaller spaces. The most

delicate part of the engine is the gear reducer, subjected to intense stress.

### 2.1.2 Turboshaft

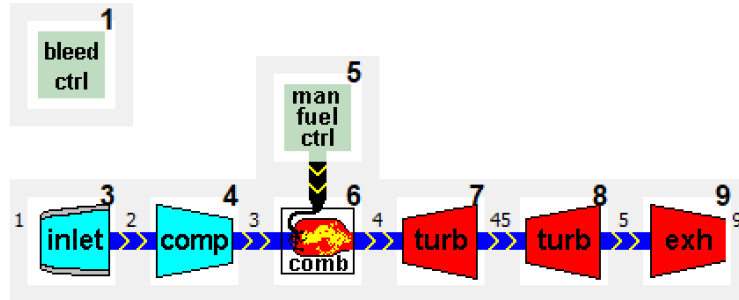


Figure 2.3. Turboshaft in GSP

A turboshaft engine is a form of gas turbine that is optimized to produce shaftpower rather than jet thrust. Conceptually, turboshaft engines are very similar to turboprops, with only minor differences.

Turboshaft engines are commonly used in applications that require a sustained high power output, high reliability, small size, and light weight. These include helicopters, auxiliary power units, boats and ships, tanks and hovercraft.

A turboshaft engine may be made up of two major parts assemblies: the 'gas generator' and the 'power section'.

The gas generator consists of a compressor, a combustion chamber with ignitors and fuel nozzles, and one or more stages of turbine. The power section consists of additional stages of turbines, a gear reduction system, and the shaft output. The gas generator creates the hot expanding gases that drive the power section.

In most designs, the gas generator and power section are mechanically separated such that they can each rotate at different speeds appropriate for the conditions. This configuration is called "free power turbine" and can be an extremely useful design feature for vehicles, as it allows the design to forgo the weight and cost of complex multiple-ratio transmissions and clutches.

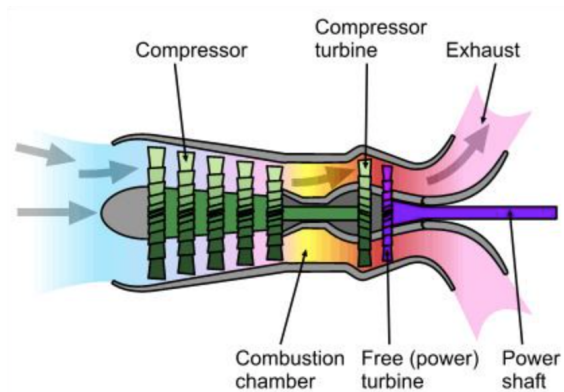


Figure 2.4. Turboshaft

### 2.1.3 Turbojet

The turbojet is an airbreathing jet engine, typically used in aircraft. It consists of a gas turbine with a propelling nozzle.

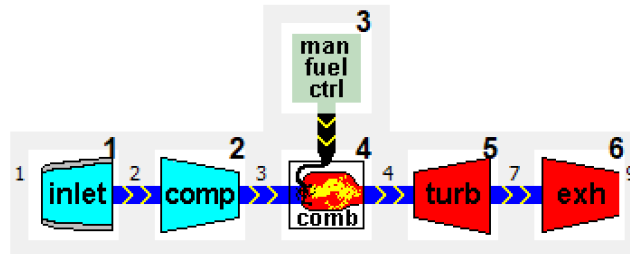


Figure 2.5. Turbojet in GSP

The gas turbine has an air inlet, a compressor, a combustion chamber, and a turbine (that drives the compressor). The compressed air from the compressor is heated by a burning fuel in the combustion chamber and then allowed to expand through the turbine. The turbine exhaust is then expanded in the propelling nozzle where it is accelerated to high speed to provide thrust.

In operation, turbojets typically generate thrust by accelerating a relatively small amount of air to very high supersonic speeds, whereas turbofans accelerate a larger amount of air to lower transonic speeds. Turbojets have been replaced in slower aircraft by turboprops because they have a better specific fuel consumption. At medium speeds, where the propeller is no longer efficient, turbojets have been replaced by turbofans. The turbofan is quieter and has better range-specific fuel consumption than the turbojet. Turbojets can be highly efficient for supersonic aircrafts. Turbojets have poor efficiency at low vehicle speeds, which limits their usefulness in vehicles other than aircraft.

Turbojets were used on Concorde and the longer-range versions of the TU-144 which were required to spend a long period travelling supersonically. Turbojets are still common in medium range cruise missiles, due to their high exhaust speed, small frontal area, and relative simplicity. They are also still used on some supersonic fighters such as the MiG-25, but since they spend little time travelling supersonically, they employ turbofans and use afterburners to raise exhaust speed for supersonic sprints.

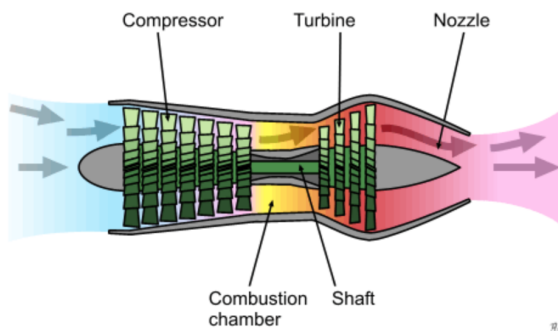


Figure 2.6. Turbojet

### 2.1.4 Turbofan

The turbofan is a type of airbreathing jet engine that is widely used in aircraft propulsion. The word "turbofan" is a portmanteau of "turbine" and "fan": the turbo portion refers to a gas turbine engine which achieves mechanical energy from combustion, and the fan to a ducted fan that uses the mechanical energy from the gas turbine to accelerate air rearwards. Therefore, whereas all the air taken in by a turbojet passes through the turbine (through the combustion chamber), in a turbofan some of that air bypasses the turbine. A turbofan can hence be thought of as a turbojet being used to drive a ducted fan, with both of these contributing to the thrust.

The ratio of the mass-flow of air bypassing the engine core divided by the mass-flow of air passing through the core is referred to as the bypass ratio. The engine produces thrust through a combination of these two portions working together; engines that use more jet thrust relative to fan thrust are known as low-bypass turbofans, conversely those that have considerably more fan thrust than jet thrust are known as high-bypass. Most commercial aviation jet engines in use today are of the high-bypass type. Afterburners are not used on high-bypass turbofan engines but may be used on either low-bypass turbofan or turbojet engines.

#### Separate flow turbofan

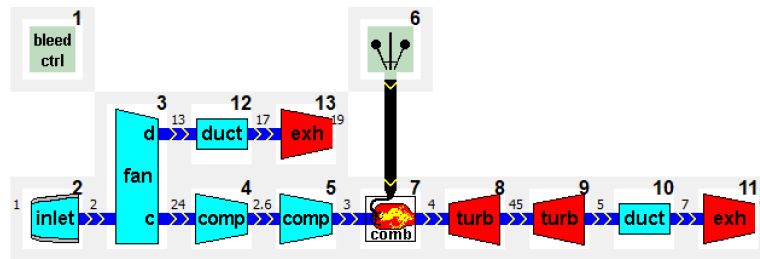


Figure 2.7. Separate flow turbofan in GSP

Their large thrust and lower consumption made turbofans with a high dilution ratio indispensable for civil use.

A schematic representation of a separate flow turbofan is shown in the figure. Downstream of the diffuser (air intake), common to the entire air flow (main and secondary), there are some compressor stages that make up the fan and are also crossed by the entire air flow. From this point on, the two flows follow different paths.

In particular, the secondary flow will not be further compressed, while the primary flow will be compressed by the compressor which develops a compression ratio (ratio between outlet pressure and inlet pressure) higher than that of the fan and is therefore characterized by several stages. This flow rate evolves successively, as in the simple turbojet, until the exit from the first turbine.

The first turbine is in fact the one that provides the power needed to move the compressor.

Downstream of the first turbine, the burnt gases, at high temperature and at an even higher pressure than atmospheric pressure, are further expanded in the second turbine, which provides the power necessary to move the fan (often referred to by the English term fan). Only downstream of the second turbine will the main flow be accelerated, exploiting the fraction of useful power still available to produce thrust.

The secondary flow downstream of the fan can be accelerated into a nozzle. Often, especially in the case of high secondary flow rates, to save weight and bulk and to limit friction, the secondary jet nozzle is positioned just downstream of the fan.

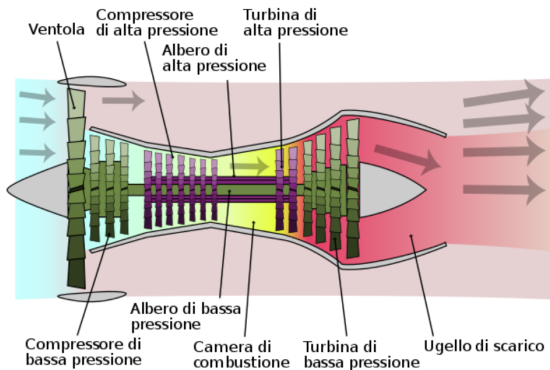


Figure 2.8. Separate flow turbofan

### Turbofan with mixer

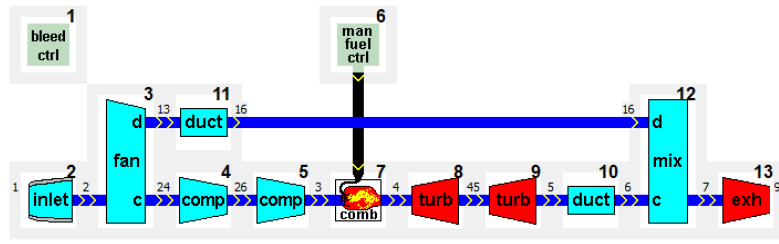


Figure 2.9. Mixer turbofan in GSP

The first turbojets complained of a very high consumption, while the pressure of the whole cycle, as well as the internal temperature, were very limited by the technology of the time. More advanced materials and the introduction of the double supercharger adopted by engines such as the Pratt & Whitney JT3C, increased the sustainable pressures and thermodynamic efficiency of the engine, but led to very poor propulsive efficiency, since turbojets generally had a small mass flow and a large discharge rate.

Low-dilution-ratio turbofans were designed to improve propulsive efficiency by reducing jet speed to values closer to flight speeds. Civilian turbofans of the 1960s, such as the Pratt & Whitney JT8D and Rolls-Royce Spey possessed a  $BPR=1$ .

In a turbofan with separate flows, the two jets are characterized by different temperatures. Since the discharge speed is proportional to the square root of the total temperature of the flow with the same pressure jump, it is possible to try to increase the temperature of the secondary flow thanks to the high temperature of the primary one. This principle is at the basis of the realization of the turbofan with associated flows which, by redistributing between the two flows not only the useful work but also the thermal energy, allows to obtain superior performances compared to the case of the turbofan with separate flows, even

if to obtain such advantage the additional weight required must be taken into account.

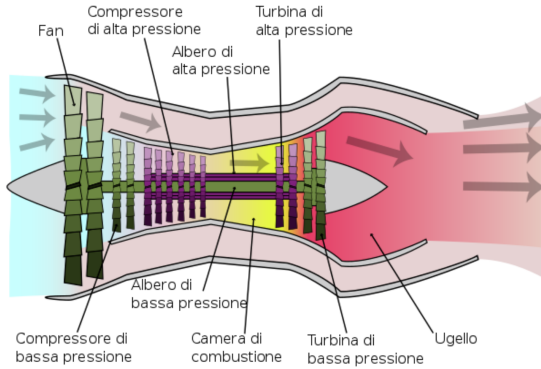


Figure 2.10. Turbofan with mixer

In an associated flow turbofan the cold flow, after being compressed, is mixed with the hot one. There is therefore a new component, the mixing chamber, where the two flows are precisely mixed before being expanded in a single nozzle. An additional constraint must be considered, compared to the case of the turbofan with separate flows. In fact, at the entrance of the mixing chamber the two flows must have the same static pressure. This means that, in the design phase, the fan compression ratio and the dilution ratio cannot both be chosen arbitrarily.

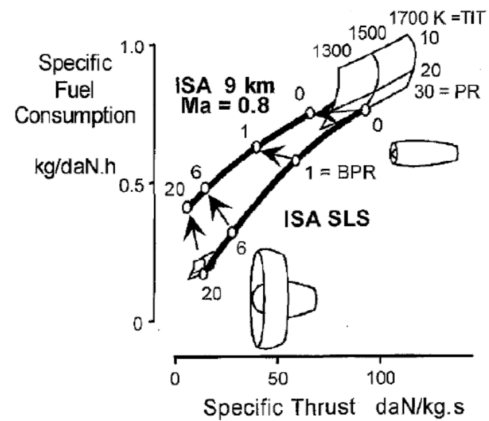
## 2.2 Decreasing consumption

To decrease the specific TSF consumption of an aircraft engine, one can act on the propulsive efficiency and/or the thermal efficiency, which make up the overall efficiency.

$$\eta_0 = \eta_p \eta_{th}$$

The thermal efficiency of a real Joule cycle can be increased, within certain limits, by increasing the maximum temperature of the cycle (and therefore the *TIT*, Turbine Inlet Temperature) and/or the compression ratio (*OPR*, Overall Pressure Ratio).

The increase of the *TIT* is limited by the organic resistance of the materials (the turbine bears very strong loads at high temperatures and *rpm*). In conventional compressor configurations, the increase in *OPR* is a function of the stage compression ratio that can be achieved. These values are around 1.2-1.3 for axial compressor stages.



A higher outflow speed allows to obtain a higher specific thrust, while the propulsive efficiency increases by decreasing the outflow speed ( $w_e$ ). [24] The outflow speed is also

linked to  $TIT$  and  $OPR$ . In fact:

$$w_e = \sqrt{2(h_e^0 - h_e)} = \sqrt{2c_p T e^0 \left[ 1 - \left( \frac{p_e}{p_e^0} \right)^{\frac{\gamma-1}{\gamma}} \right]}$$

Total temperature  $T^0$  and  $P^0$  are functions of the  $TIT$  and the  $BPR$ . It is therefore necessary to try to decouple the system by introducing another degree of freedom. This is what happens in the case of double-flow machines, in turbofans: a core flow with high thermal efficiency is associated with a cold flow with high propulsive efficiency.

So, in conclusion, the thermal efficiency increases with  $TIT$  and  $OPR$ , while the propulsive efficiency increases with the value of  $BPR$ .

The choice of the thermodynamic cycle and engine architecture affects emissions. The pressure and temperature levels have different effects on various pollutants. Low specific consumption (low fuel consumption) and high specific thrusts (low weight engine) reduce  $CO_2$  and  $H_2O$  emissions. High  $TIT$  temperatures increase  $NO_x$ . [24]

## 2.2.1 Changes to improve performance to classic architecture

### Intercooled recuperative core

This solution aims at a high specific thrust and low fuel consumption, through the introduction of intercooling and energy recovery of the exhaust gases. The compression process is divided into two stages, between which the fluid is refrigerated, thus reducing the compression work compared to the non-refrigerated case.

With the same  $TIT$  temperature entering the turbine system, the lower compression work translates into an increase in the enthalpy gap available downstream of the turbines, and therefore in a potential increase of specific thrust. [24] To obviate the decrease in thermal efficiency, a regeneration is also introduced.

By means of an exchanger, part of the heat from the exhaust gases to the turbine is transferred to the fluid upstream of the combustion chamber, thus reducing the amount of energy to be supplied to reach a certain end-of-combustion temperature.

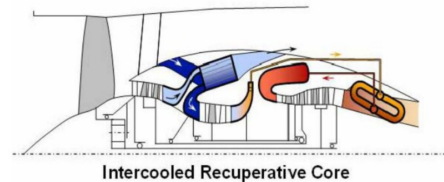


Figure 2.11. Intercooled recuperative core

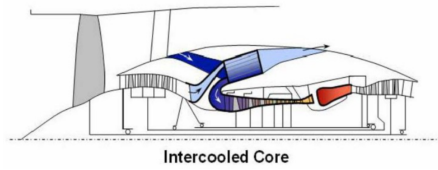


Figure 2.12. Intercooled core

### Intercooled core

The intercooling is applied between LPC and HPC which allows to increase the overall compression ratio with the same compression work. This could reduce specific thrust  $SFC$  and  $NO_x$ . Innovative solutions are being studied for lightweight intercoolers and high efficiency HPC compressors.

### Active core

The project aims at the development of new active systems to increase the thermal efficiency through active or semi-active control of the HPC, increase the overall efficiency of the thruster by controlling the cooling of the turbine in all flight phases.[24]

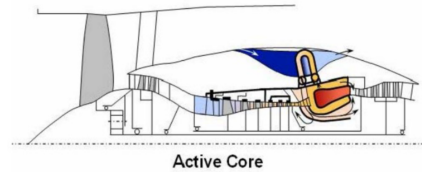


Figure 2.13. Active core

It is therefore possible to increase the stall margin both at low rpm and at high rpm by controlling the first or last stages of the high pressure compressor. This translates into the possibility of raising the operating line of the compressor map and taking us to areas with higher yields.

### Flow Controlled Core

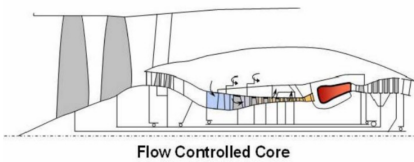


Figure 2.14. Flow Controlled Core

This solution is characterized by a high bypass ratio, therefore it requires a compact high pressure compressor with a high compression ratio to compensate for the low pressure increase in the fan and in the low pressure compressor. Here, too, an active flow control system allows to obtain a high efficiency and increased stability of the compressor. [24]

### Interstage Turbine Burner

In traditional turbine engines, the fuel is burned in the single combustor before expansion takes place into the turbine. The Continuous Turbine Burner (CTB) concept assumes a second combustion in the turbine, without the introduction of additional components. Similarly to what happens in the Carnot cycle, the heat supply occurs at a constant temperature.

In the ideal case, the heat would be supplied to the fluid during expansion in the turbine, at a constant temperature, which is technically difficult to achieve.

The alternative is to introduce an Interstage Turbine Burner (ITB), which carries out a second combustion in the transition duct between the HPT and LPT turbine stages, without the introduction of additional components.

Note that unlike what happens in the post-combustor, with the ITB heat is supplied to the fluid astride the turbines, at higher pressure levels than the first.

The main advantages linked to the use of the ITB, placed in the transition zone between the high pressure and low pressure turbine stages, are the increase in the specific thrust and the reduction of the  $NO_x$  emission, consequent to a decrease in maximum cycle temperature.[24]

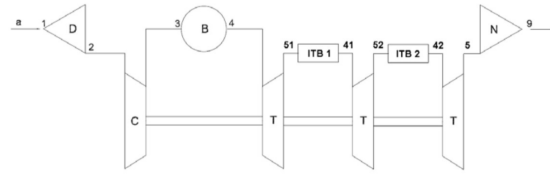


Figure 2.15. Interstage Turbine Burner

## 2.3 Innovative technologies and architectures

In recent years, new innovative solutions have been studied to reduce the consumption of civil and commercial aircraft.

This is the case of the *Partially Turboelectric*, where the energy moves from fuel to turbofan, the engine produces thrust and power for the electric generators. Then, the electric power goes to electric motors to drive other fans. This configuration expects a reduction of fuel burn of 12%.

Another configuration is the *Partially Turboelectric with fuel cell*, which differs from the previous one as in this case the energy obtained from the fuel goes to turbofans and to solid oxide fuel cell. A saving of 50% is expected.

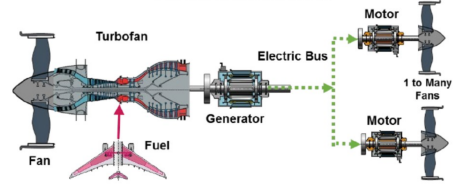


Figure 2.16. Partially Turboelectric

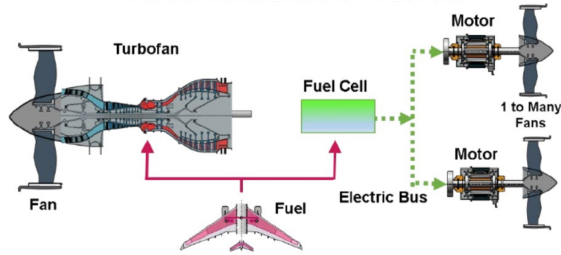


Figure 2.17. Partially Turboelectric-fuel cell

A similar type of structure can be obtained if there were a turboshaft instead of a turbofan. In this case turboshaft doesn't produce thrust, but only energy for the electric generator.

In *Parallel Hybrid*, instead, energy to turboshaft comes from both fuel and batteries. The electric power goes to electric motors (may be superconducting with a cryogenic power management system) to

boost the turbofan. In this case the fuel saving coincides with the energy that can be introduced.[24]

The most important innovative architecture for this work is *Hydrogen Combustion*. In this engine there is high power density, in less volume. The  $CO_x$  emissions, as explained, are zero, but there is a great amount of water vapor. Moreover, the combustion of hydrogen is highly flammable, and the high flame speed increases the danger of flashback. [24]

Hydrogen can be used as aircraft fuel when it is burned in an  $H_2$  combustion engine or reacted in a fuel cell that powers electric motors. Despite three times the gravimetric energy density of kerosene, the relatively higher volume of hydrogen requires a larger volume, which requires larger tanks on board the aircraft and suitable aircraft designs. The size and weight of  $H_2$  tanks place

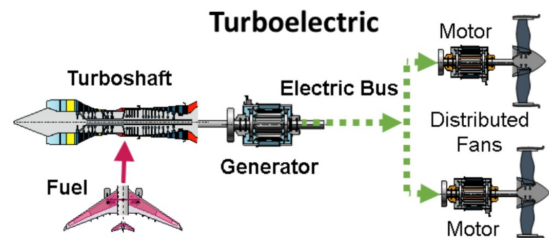


Figure 2.18. Turboelectric

major limitations on the high energy demand on long-haul flights, potentially reducing costs significantly for long-haul aircraft.

As for the tanks installed on board the aircraft, hydrogen can be stored as pressurized gas or in liquid form. While gaseous storage may be suitable for shorter flights and is commercially available, this study focuses on liquid hydrogen ( $LH_2$ ) storage tanks as they require about half the volume and, as a result, are significantly lighter than tanks for gaseous hydrogen. Compared to kerosene,  $LH_2$  tanks are still about four times larger. Since  $LH_2$  must remain cold and heat transfer must be minimized to avoid vaporization of hydrogen, spherical or cylindrical tanks are required to keep losses low. To efficiently integrate the tanks into the aircraft fuselage, the airframe will need to be extended, which increases the aircraft's operational empty weight.

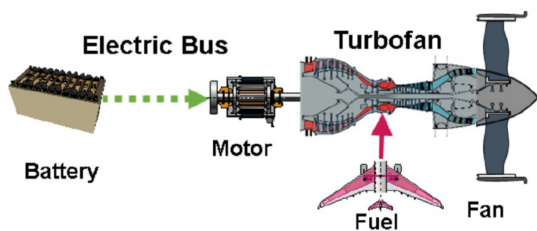


Figure 2.19. Parallel Hybrid

The tanks can then be subjected to a stress due to the fact that it is desirable to keep the pressure inside the tanks at an approximately atmospheric value, instead of letting it descend to the ambient value at high altitude (because the boiling temperature of liquid hydrogen drops further as pressure decreases). The tank walls must therefore resist the difference between internal and external pressure, which implies the need to adopt thicker, therefore heavier, walls. These bulky tanks could be housed

at the top of the fuselage. [24]

This arrangement is chosen because any fuel leaks, which could give rise to flames in contact with the air, would quickly move away upwards (thanks to the lightness of the hydrogen), without risk for passengers.

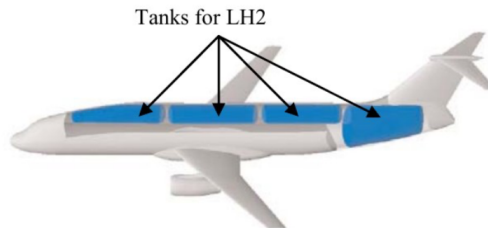


Figure 2.20. Possible arrangement of  $LH_2$  tanks

Still on the subject of safety in the event of fire, it should be noted that in fatal air accidents (in conventional aircraft) about 80% of deaths are caused by fires and consequent formation of toxic fumes (which are released in the combustion of kerosene). The adoption of hydrogen as fuel would therefore make it possible to drastically reduce these losses of human life.

Also of great importance is the  $LH_2$  fuel system for distributing, vaporizing and feeding  $LH_2$  to fuel cells or turbines. Indeed,  $LH_2$  requires cryogenic cooling up to 20 Kelvin degrees. These temperatures must be managed by pipes, valves and compressors. The boil-off must be kept low and material losses and fragility are avoided.

In a fuel cell powered airplane, hydrogen is converted into electricity which then drives an electric motor and a fan or propeller. The most advanced and suitable for aviation today are low temperature proton exchange membrane (PEM) fuel cells. Adding an energy storage such as a battery to this system helps ensure rapid load follow-up and reduction of power peaks to optimize fuel cell system sizing. [1]

In  $H_2$ -burning airplanes,  $LH_2$  is directly burned in a turbine, just like kerosene, to create thrust. The use of cryogenic fuel cooling is expected to slightly increase efficiency (40 to 50% less calorific value) with respect to conventional engines.

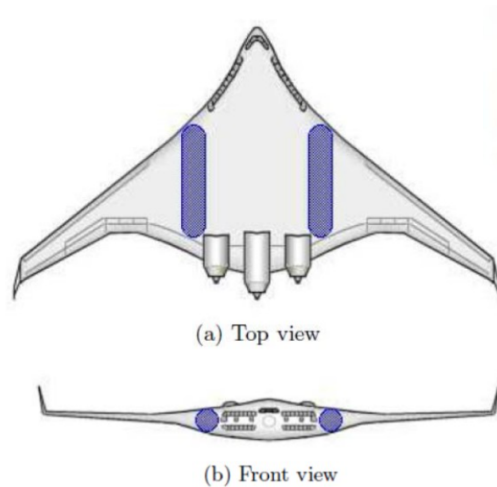


Figure 2.21. Possible arrangement of  $LH_2$  tanks



## Chapter 3

# Data analysis for subsonic flight

In this chapter will be analyzed the ICAO database, which collects data on the emissions and consumption of many engines during their LTO cycle.

In the Emissions Databank is described the identification number of each engine, the engine manufacturer, and obviously the engine type ( $TF$  = turbofan,  $MTF$  = mixed turbofan). For each engine can be found the *Bypass Ratio*  $BPR$ , *Overall Pressure Ratio*  $PR$ , *maximum rated Thrust*  $T$  [ $kN$ ], and many other technical information. Moreover, a lot of data about emissions are collected. For example there are the values of hydrocarbon emissions during different phases of the mission: take off, climb, approach and idle (expressed in  $g/kg$ ). As for hydrocarbons, the same data are reported for carbon monoxide, nitrogen oxides and smoke number. Also the fuel flow used during the LTO cycle (expressed in  $kg/sec$ ).

Having this big amount of data (about 600 engines), it was possible to try to relate the different variables and seek a relationship at experimental level. Dividing the engines between separate flow turbofans and mixer turbofans the independent variables used are:

- Bypass Ratio  $BPR$ ;
- Pressure Ratio  $PR$ ;

and the dependent ones:

- total emission of carbon monoxide during LTO cycle  $CO$  in  $g/kg$
- total emission of hydrocarbons during LTO cycle  $HC$  in  $g/kg$
- total emission of nitrogen oxides during LTO cycle  $NO_x$  in  $g/kg$

### 3.1 Fourth degree polynomial

Initially we tried to find a relationship between the different variables using the classic matlab functions: spline, polyfit and polyval, considering a fourth degree polynomial.

Using the `xlsread` function it was possible to read each column of the ICAO excel document and to save the data useful for the analysis. Then, once the data between turbofan with separate flows and turbofan with mixer were divided, a correlation between the different variables was searched, in order to try to insert them in a graph.

```
bpr=xlsread('dati_motori', 'G2:G619'); %BPR
for i=1:length(arc)-1
    s2='TF';
    tf(i)= strcmp(arc(i),s2);
    if tf(i)==1
        BPR(i)=bpr(i);
    elseif tf(i)==0
        BPR(i)=0;
    end
end %legge le righe riferite a turbofan a flussi separati
```

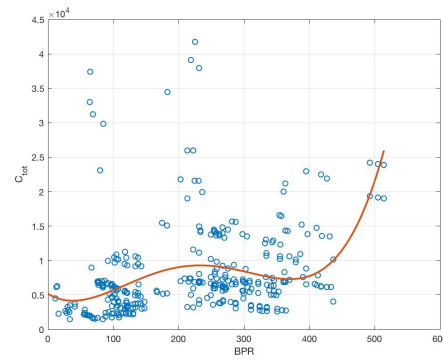
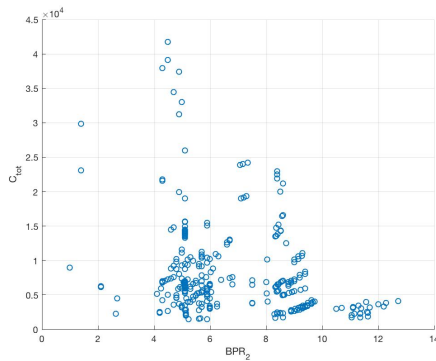
Figure 3.1. Matlab code for reading data

```
figure(1) %Spinta
y=C_tot2;
x=T2;
c= polyfit(x, y, 4);
xx=linspace(0,514,456);
pp=polyval(c,xx);
plot(x,y,'o',xx,pp)
title('T,C_{tot}')
hold on
```

Figure 3.2. Matlab code for plot

The obtained graph resulted in a distribution of points, so the objective was to look for a function that would approximate and describe the phenomenon. The functions `polyfit` and `polyval` were used. `polyfit(x,y,n)` returns the coefficients for a polynomial  $p(x)$  of degree  $n$  that is a best fit (in a least-squares sense) for the data in  $y$ , while `polyval(p,x)` returns the value of a polynomial of degree  $n$  evaluated at  $x$ .

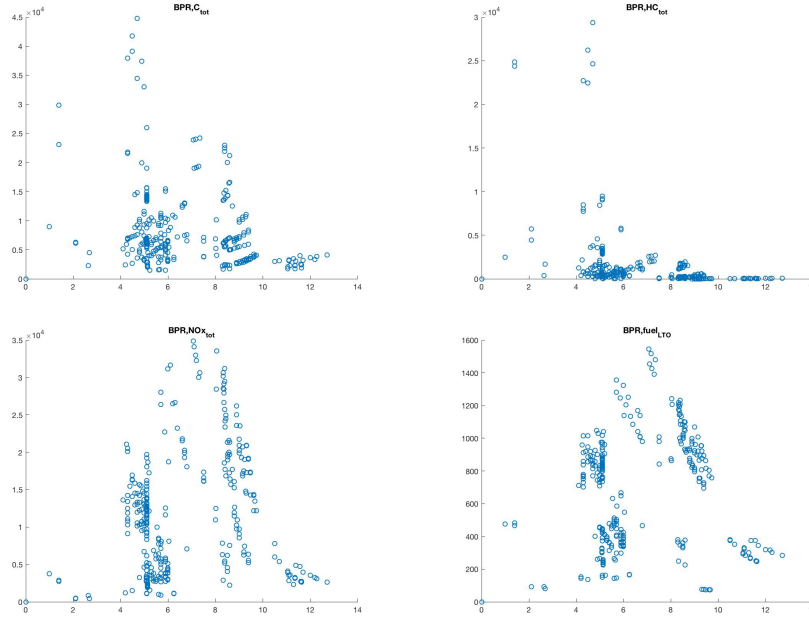
A fourth degree polynomial was used in order to better approximate the distribution of the points, but without having an excessively high degree of the polynomial.



### 3.1.1 Turbofan separated flow

This section shows all the graphs obtained through this method. Furthermore, each curve is associated with the fourth degree function that describes it.

## Bypass Ratio

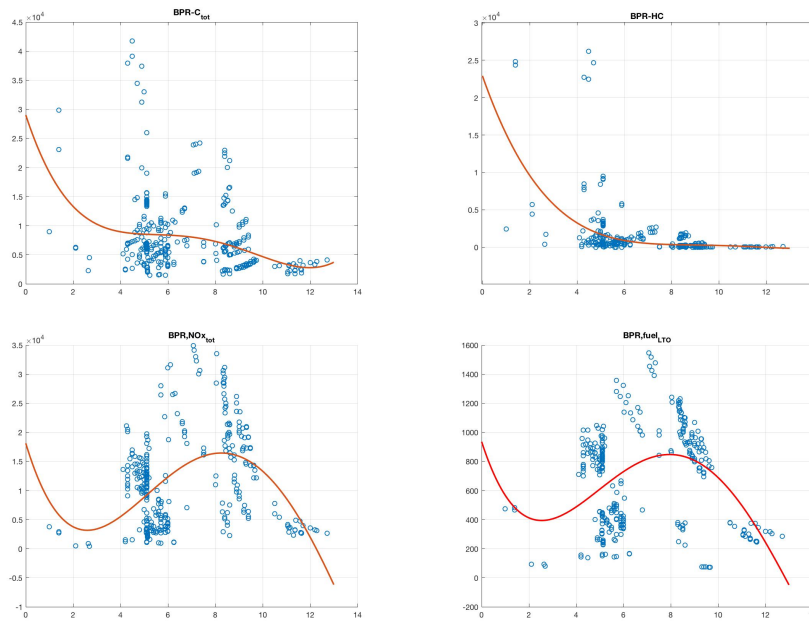


$$\text{BPR-C} \rightarrow 9x^4 - 260x^3 + 2742x^2 - 12367x + 29013$$

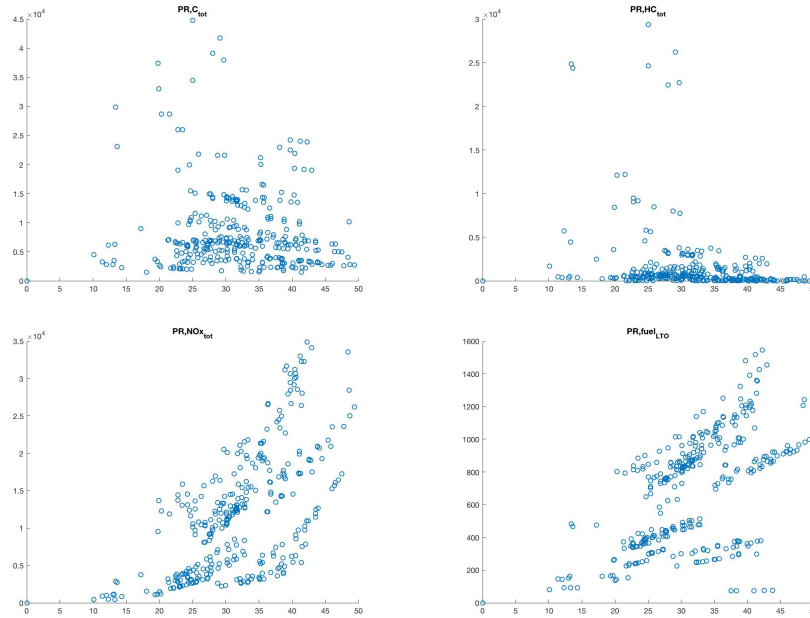
$$\text{BPR-HC} \rightarrow 2x^4 - 88x^3 + 1338x^2 - 9001x + 22914$$

$$\text{BPR-NOx} \rightarrow 9x^4 - 335x^3 + 3779x^2 - 13464x + 18113$$

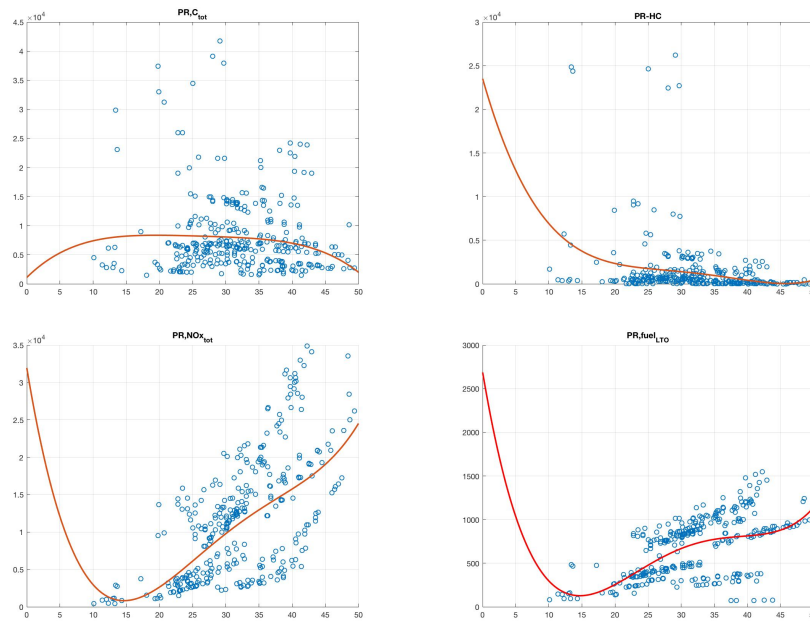
$$\text{BPR-fuel} \rightarrow 0,37x^4 - 13,4x^3 + 144,9x^2 - 500,8x + 935,062$$



## Pressure Ratio

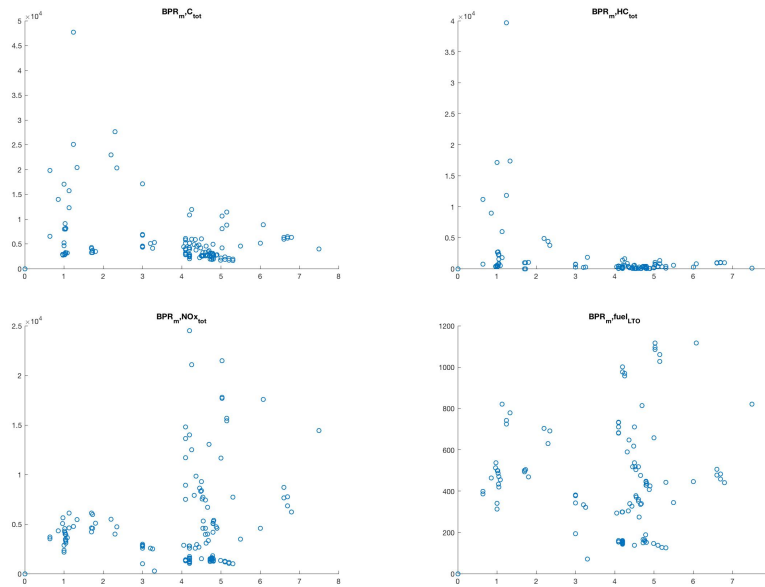


$$\begin{aligned} \text{PR-C} &\rightarrow 1,6x^3 - 63,9x^2 - 1124,9x + 1089,3 \\ \text{PR-HC} &\rightarrow -3x^3 + 124x^2 - 2660x + 23510 \\ \text{PR-NOx} &\rightarrow 7x^3 + 307x^2 - 5354x + 31942 \\ \text{PR-fuel} &\rightarrow -0,6x^3 + 26,6x^2 - 448,7x + 2686,4 \end{aligned}$$



### 3.1.2 Turbofan with mixer

#### Bypass Ratio

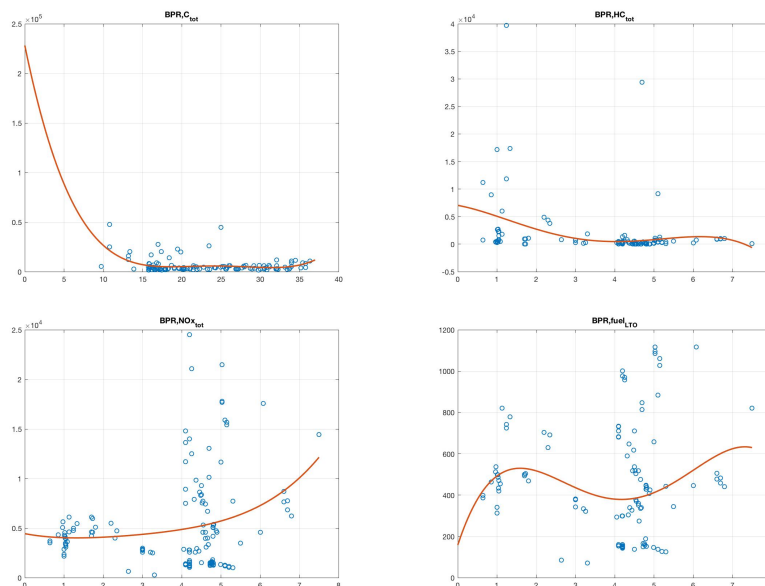


$$\text{BPR-C} \rightarrow -70x^4 + 1175x^3 - 6298x^2 + 10899x + 4474$$

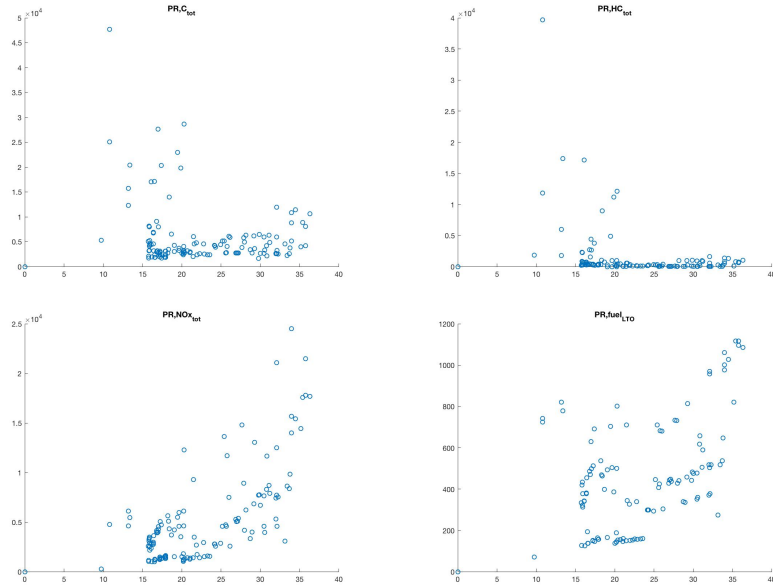
$$\text{BPR-HC} \rightarrow -24,5x^4 + 316,5x^3 - 954,1x^2 - 1320,9x + 7043,2$$

$$\text{BPR-NO}_x \rightarrow 7,9x^4 - 84x^3 + 426,2x^2 - 757,8x + 4442,8$$

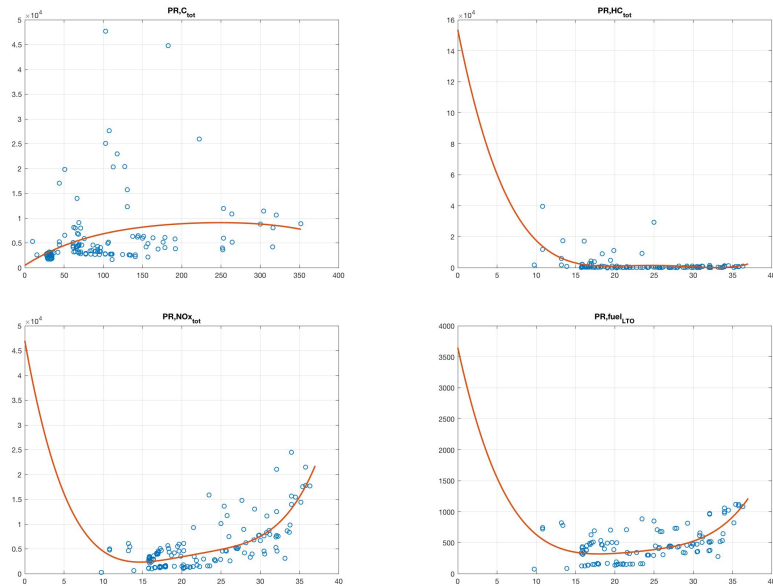
$$\text{BPR-fuel} \rightarrow -2,96x^4 + 51,59x^3 - 288,64x^2 + 573,94x + 18,43$$



## Pressure Ratio



$$\begin{aligned} \text{PR-C} &\rightarrow 70x^3 + 2450x^2 - 38570x + 228210 \\ \text{PR-HC} &\rightarrow 40x^3 + 156x^2 - 2544x + 15354 \\ \text{PR-NOx} &\rightarrow -20x^3 + 642x^2 - 89034x + 46987 \\ \text{PR-fuel} &\rightarrow -1,1x^3 + 37,9x^2 - 583,7x + 3648,1 \end{aligned}$$



## 3.2 Curve fitting

A more optimized model was then used to carry out this study: the Curve Fitting. With this Tool in Matlab App, is possible chosen among various functions to represent and interpolate data. After having chosen the function, and set the parameters, Matlab returns the errors and results.

The 2-3 variables to be analyzed and the name of the interpolation curve are selected. Then the data approximation function is selected: each one has characteristics or parameters that can be modified at will, if necessary.

There are many possible functions that can be implemented in order to interpolate the entered data:

- Exponential
- Fourier
- Gaussian
- Interpolant
- Linear Fitting
- Polynomial
- Power
- Rationall
- Smoothing Spline
- Sum of Sine
- Weibull

All these functions are obviously adaptable to the different specific cases. In fact, for example, it is possible to select the degree of polynomials or the degree of power.

The results obtained are:

- *RMSE*: Root Mean Squared Error, the most important datum; it represents the square root of the mean of the difference between model prediction and target value (look for smaller values);
- *R-Squared*: indicates the proportionate amount of variation in the response variable  $y$  explained by the independent variables  $x$  in the linear regression model. The larger the R-Squared is, the more variability is explained by the linear regression model (look for R-squared close to 1);
- *SSE*: Standard Deviation is a statistical dispersion index, which is an estimate of the variability of a population of data or a random variable. It is one of the ways to express the dispersion of data around a position index;
- *Adjusted R – Squared*

Once the model has been selected, it is possible to use the  $yfit = name.predictFcn(x)$  function in the workspace, so as to insert a value of the independent variable and obtain, through the selected regression model, the corresponding value of the dependent variable.

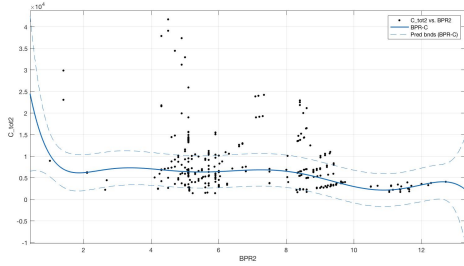
It is necessary to highlight that the analysis carried out and the obtained graphs are only a basis on which to develop assumptions and to have reference values that can be compared with the analysis in the supersonic field. They were not suitable for a specific study on a subsonic motor model.

### 3.2.1 Turbofan separated flow

By Pass Ratio

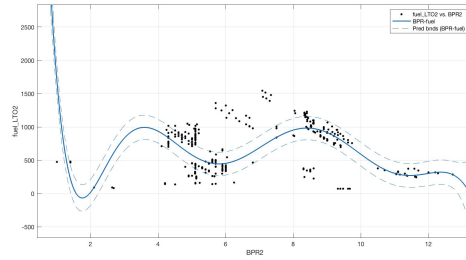
$$BPR - C$$

Polynomial-LAR, eighth grade  
 R-Squared=0,8663  
 RMSE=2260



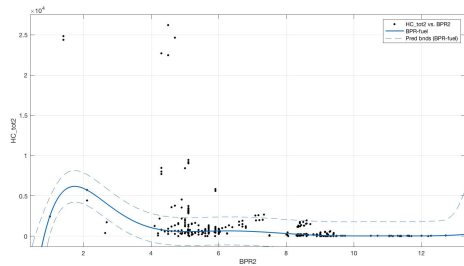
$$BPR - fuel$$

Polynomial-LAR, eighth grade  
 R-Squared=0,896  
 RMSE=105,8



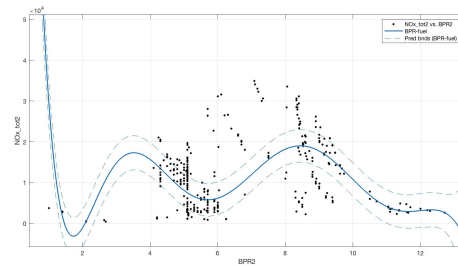
$$BPR - HC$$

Polynomial-LAR, eighth grade  
 R-Squared=0,884  
 RMSE=1048



$$BPR - NO_x$$

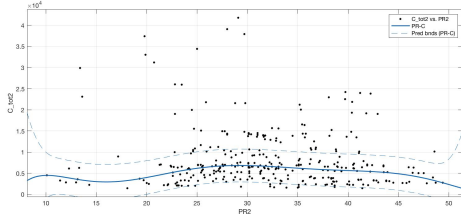
Polynomial-LAR, eighth grade  
 R-Squared=0,9046  
 RMSE=2419



Pressure Ratio

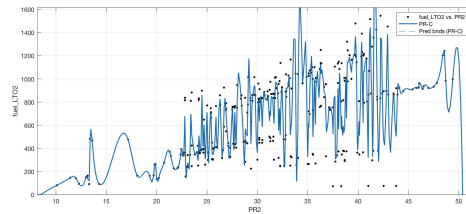
$$PR - C$$

Polynomial-LAR, eighth grade  
 R-Squared=0,8556  
 RMSE=2350



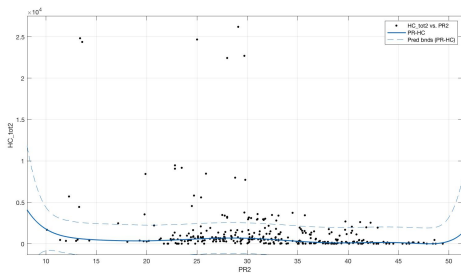
$$PR - fuel$$

Smoothing spline  
 R-Squared=0,7755  
 RMSE=202,9



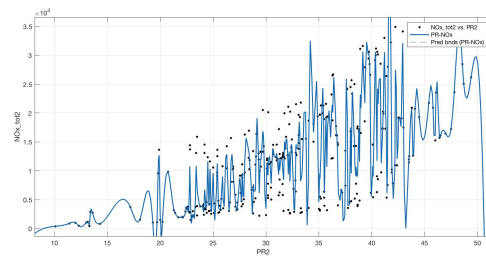
$$PR - HC$$

Polynomial-LAR, eighth grade  
 R-Squared=0,8645  
 RMSE=1123



$$PR - NO_x$$

Smoothing spline  
 R-Squared=0,8222  
 RMSE=4314

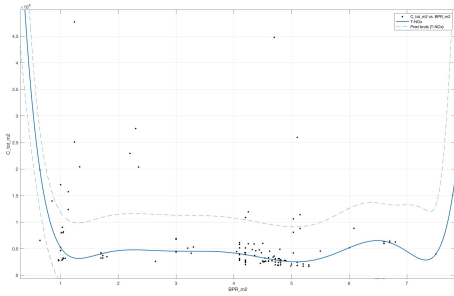


### 3.2.2 Turbofan with mixer

By Pass Ratio

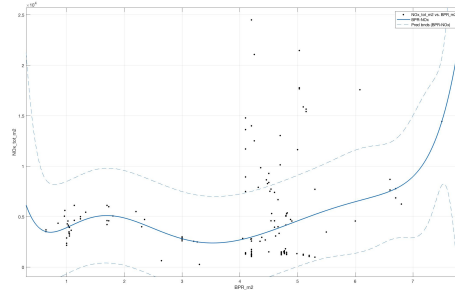
*BPR – C*

Polynomial-LAR, eighth grade  
 R-Squared=0,6963  
 RMSE=3915



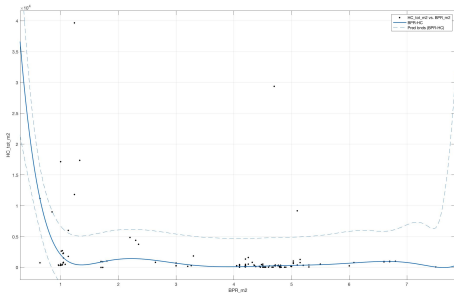
*BPR – NO<sub>x</sub>*

Smoothing spline  
 R-Squared=0,6452  
 RMSE=182,3



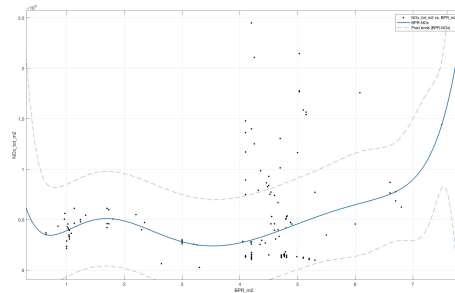
*BPR – HC*

Polynomial-LAR, eighth grade  
 R-Squared=0,6925  
 RMSE=2731



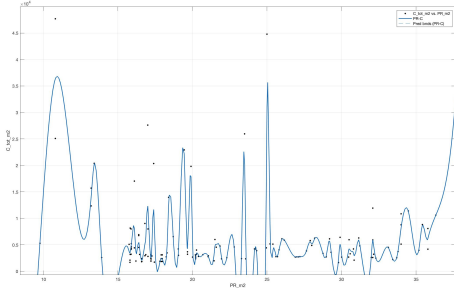
*BPR – NO<sub>x</sub>*

Polynomial-LAR, eighth grade  
 R-Squared=0,6814  
 RMSE=2699

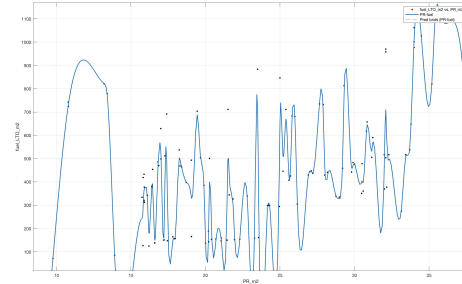


**Pressure Ratio**

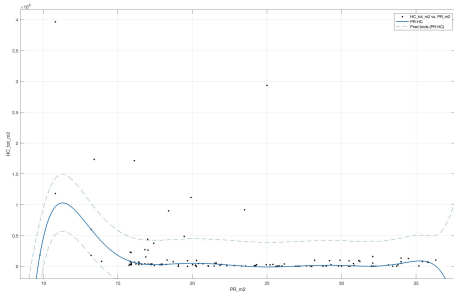
*PR – C*  
 Smoothing spline  
 R-Squared=0,8  
 RMSE=4551



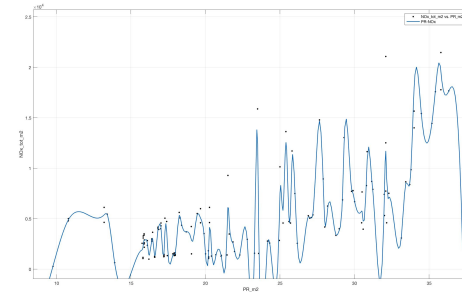
*PR – fuel*  
 Smoothing spline  
 R-Squared=0,9179  
 RMSE=107,6



*PR – HC*  
 Polynomial-LAR, eighth grade  
 R-Squared=0,7702  
 RMSE=2361



*PR – NOx*  
 Smoothing spline  
 R-Squared=0,9092  
 RMSE=2063



### 3.3 Final results

As can be seen from the graphs just presented, it is immediate to understand that there is no simple relationship between By Pass Ratio, Pressure Ratio and the different Emission Indexes.

It was therefore tried to divide the type of motors according to the nominal thrust (reported in the ICAO database).

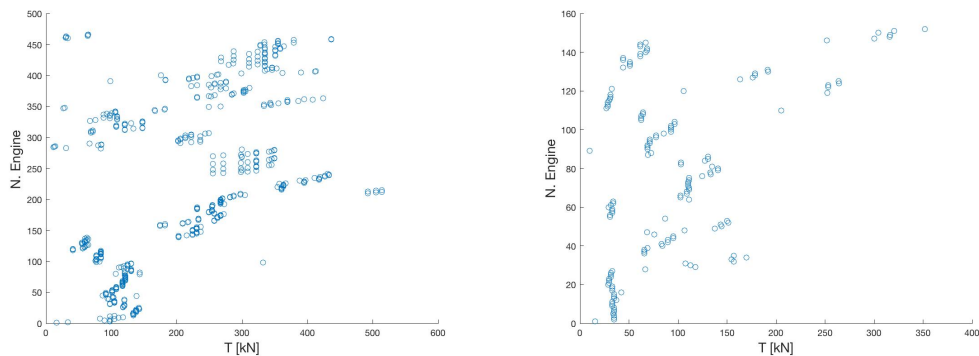
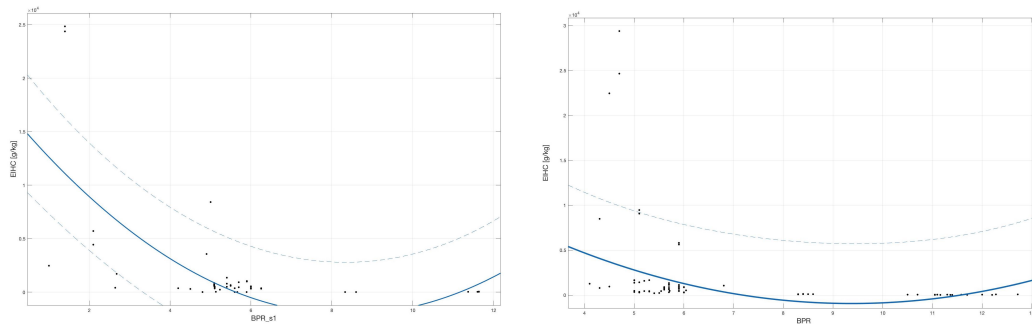


Figure 3.3. Rated thrust for turbofan separated flow and with mixer

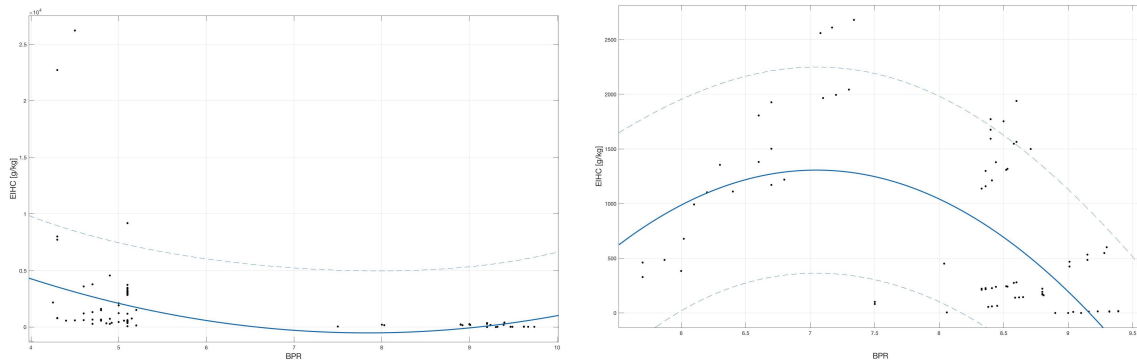
With this division into 4 intervals, new functions that could graph the trend of the Emission index as a function of  $BPR$  and  $PR$  were sought .

For simplicity, only the Emission Index values (for  $HC$ ) of the turbofan with mixer depending on the By Pass Ratio are shown below.

For  $T < 100 kN$  and for  $100 kN < T < 200kN$ :



For  $200 < T < 300 \text{ kN}$  and for  $T > 300 \text{ kN}$ :



In this case, a second degree curve was used for each "section". As can be seen even from these graphs alone, there is no univocal and precise relationship that describes the performance of the *Emission Index* as a function of the *BPR* (and the *PR*).

This reasoning was developed for the mixer turbofan and the separate flow turbofan. In both cases, with *BPR* and with *PR* there is no second degree function that can express in detail the performance of the *EIHC*, *EINO<sub>x</sub>* and *EICO*.

# Chapter 4

## Subsonic Emission Method during LTO and CCD

### 4.1 Calculation of the quantity of emissions

This section presents a model to calculate the quantity and type of emissions emitted by the engines of subsonic civil aircraft.

From the ICAO database it is possible to read the emission index data [ $\frac{g}{kg_{fuel}}$ ] for  $HC$ ,  $CO$  and  $NO_x$  in the 4 different phases of the Landing-Take off cycle.

Furthermore, there are the fuel flow [ $\frac{kg}{s}$ ] values for each of these phases: take off, climb, approach, taxi/idle. For each phase of the LTO cycle, the duration in the time interval and the percentage of nominal thrust used are known.

Phase	Time [ <i>min</i> ]	Thrust
Take-off	0.7	100% $F$
Climb	2.2	85% $F$
Approach	4.0	30% $F$
Taxi/ground idle	26.0	7% $F$

Table 4.1. Time in operating mode and thrust setting

For the calculation of the emission quantity, the following simple formula is applied:

$$Emission_{i,k} = EI_{i,k} w_{f,k} \Delta t$$

Where the subscript  $i$  corresponds to the type of emission and  $k$ , to the phase of the LTO cycle to be analyzed.

The emissions of  $H_2O$ ,  $SO_x$  and  $CO_2$  can also be analyzed. In fact, the emission indexes of these particular emissions can be considered constant, and are shown below:

$$EICO_2 = 3160 \frac{g}{kg}$$

$$EI_{H_2O} = 1240 \frac{g}{kg}$$

$$EISO_x = 0.6 \frac{g}{kg}$$

As an example we used the engine of the A380: the GP7270. The graphs obtained are shown below. It is therefore possible to analyze the emissions in each phase of the LTO cycle, and graph the data as follows:

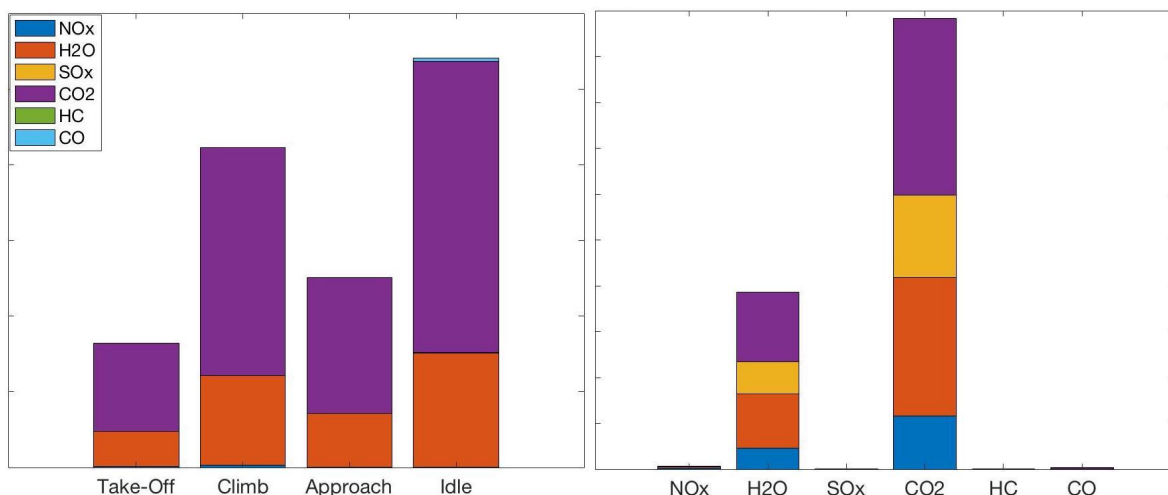


Figure 4.1. Emissions in LTO cycle

It is important to note, in the first plot, that some emissions do not seem to appear, but in reality they are only in very small quantities compared to the most present:  $CO_2$  and  $H_2O$ .

In the second figure, it is possible to see the 4 different phases of the LTO cycle: in blue *take off*, red for *climb*, yellow for *approach* and purple for *taxi*.

Emissions	Take Off	Climb	Approach	Taxi/Idle	TOT
$NO_x$ [kg]	4.62	8.98	2.20	1.91	17.71
$CO$ [kg]	0.01	0.03	0.22	12.26	12.51
$CO_2$ [t]	0.35	0.91	0.54	1.15	2.95
$H_2O$ [t]	0.14	0.36	0.21	0.45	1.16
$SO_x$ [kg]	0.07	0.17	0.10	0.22	0.56
$HC$ [kg]	0.003	0.009	0.012	1.48	1.50

Table 4.2. Summary table of results

## 4.2 Fuel Flow Method 2

The method for calculating aircraft engine emissions requires the knowledge of the engine internal gas path parameters at the high compressor exit /combustor inlet. These are total pressure  $P_3$ , total temperature  $T_3$  and, obviously, the engine fuel flow  $W_F$ . For calculating  $NO_x$  emissions is required the knowledge of ambient atmospheric humidity.

In order to obtain the emission index for  $HC$ ,  $CO$  and  $NO_x$  it is necessary to define the aircraft mission, and after that to execute a code that predicts airplane performance. The code's outputs are thrust and fuel flow in different points along the mission.

This information is then used as input to an engine performance model. This model calculates  $P_3$  and  $T_3$  for each point of the mission. Then, it is possible to use these data to calculate the emission indexes at sea level ( $EINO_{x,sl}$ ,  $EICO_{sl}$ ,  $EIHC_{sl}$ ). These reference emission indexes are therefore corrected to flight conditions using the following equations:

$$EICO_{alt} = EICO_{sl} \left( \frac{P_{3,sl}}{P_{3,alt}} \right)^x \left( \frac{FAR_{sl}}{FAR_{alt}} \right)^z$$

$$EIHC_{alt} = EIHC_{sl} \left( \frac{P_{3,sl}}{P_{3,alt}} \right)^x \left( \frac{FAR_{sl}}{FAR_{alt}} \right)^z$$

$$EINO_{x,alt} = EINO_{x,sl} \left( \frac{P_{3,alt}}{P_{3,sl}} \right)^y \left( \frac{FAR_{alt}}{FAR_{sl}} \right)^z e^H$$

The exponents  $y$  and  $x$  are combustor unique and are empirically derived by the manufacturers. The value for the  $NO_x$  pressure exponent  $y$  has been seen to range between 0.2 and 0.5. Theoretically the value of  $y$  is 0.5, while published empirical data would suggest a typical value of 0.4<sup>3</sup>. The value of exponent  $x$ , for the  $HC$  and  $CO$  pressure, is assumed to be 1.0. The exponent  $z$  is actually 0 for conventional rich front and single annular combustors and so this term drops out of the equations. The  $NO_x$  equation includes a humidity factor,  $e^H$  which was originally developed from 19 engine samples of JT9D's production. [26]

The  $P3T3$  method determines the emission indexes firstly by using the  $T_3$  at altitude in order to look for an Emission Index at sea level, and then applying a pressure correction. Using the  $P3T3$  method requires deep knowledges of aircraft engine and access to proprietary performance models. It is therefore necessary to use a different method to be able to calculate the emission index. A method based on the most commonly available non proprietary indicator of engine power setting was pursued, the engine fuel flow. Engine power in flight can be known as fuel flow, therefore if a means can correlate  $T_3$  and fuel flow then a basis for a "Fuel Flow Method" could be investigated.

Therefore emissions are correlated with  $T_3$  and then a pressure correction is applied. The first method was called "Fuel Flow Method 1", but, compared to  $P3T3$  method, an improved approach was necessary. This variation from Fuel Flow Method 1 is based on an energy balance across the combustor that shows that it exists a fuel flow correlation essentially represents the difference in airflow rates through the combustor between sea level and flight conditions. [26]

### Derivation

The first step in order to derivate the Fuel Flow Method 2 is to calculate the pressure correction. The compression process between freestream and combustor inlet is assumed as isentropic.

$$\frac{T_3}{T_1} = \left( \frac{P_3}{P_1} \right)^{\frac{\gamma-1}{\gamma}}$$

$$T_3 = T_1 \left( \frac{P_3}{P_1} \right)^{\frac{\gamma-1}{\gamma}}$$

At flight condition:

$$T_{3,alt} = T_1 \left( \frac{P_{3,alt}}{P_{1,alt}} \right)^{\frac{\gamma-1}{\gamma}}$$

And at sea level conditions:

$$T_{3,sl} = 518.67 \left( \frac{P_{3,sl}}{14.696} \right)^{\frac{\gamma-1}{\gamma}}$$

In the P3T3 emissions prediction methodology  $T_{3,sl} = T_{3,alt}$   
Therefore it is possible to write the previous equations:

$$T_1 \left( \frac{P_{3,alt}}{P_{1,alt}} \right)^{\frac{\gamma-1}{\gamma}} = 518.67 \left( \frac{P_{3,sl}}{14.696} \right)^{\frac{\gamma-1}{\gamma}}$$

$$\frac{P_{3,alt}}{P_{3,sl}} = \frac{\delta_1}{\theta_1^{\frac{\gamma-1}{\gamma}}}$$

A correlation between total to static pressure and temperature ratios for the compressible flow:

$$\beta = 1 + \frac{\gamma - 1}{2} M^2$$

Using this function, the equations can be re-written as

$$\frac{P_{3,alt}}{P_{3,sl}} = \frac{\delta_{amb}\beta}{(\theta_{amb}\beta)^{\frac{\gamma-1}{\gamma}}} = \frac{\delta_{amb}}{\theta_{amb}^{\frac{\gamma}{\gamma-1}}}$$

If the value of  $\gamma$  is 1.4:

$$\frac{P_{3,alt}}{P_{3,sl}} = \frac{\delta_{amb}}{\theta_{amb}}^{1.5}$$

Using the polytropic efficiency  $\eta_p$  to describe the compression from the freestream to the combustor inlet, implies:

$$\frac{T_3}{T_1} = \frac{P_3}{P_1}^{\frac{\gamma-1}{\gamma\eta_p}}$$

$$\frac{P_{3,alt}}{P_{3,sl}} = \frac{\delta_{amb}}{\theta_{amb}^{\frac{\gamma_p}{\gamma-1}}}$$

Substituting the gamma value and a typical polytropic efficiency value ( $\gamma=1.38$  e  $\eta_p=0.9$ ):

$$\frac{P_{3,alt}}{P_{3,sl}} = \frac{\delta_{amb}^{3.3}}{\theta_{amb}}$$

An empirically modification was made to the exponent of  $\delta_{amb}$  to better collapse the data and results in the following pressure correction:

$$\frac{P_{3,alt}}{P_{3,sl}} = \frac{\delta_{amb}^{1.02 \cdot 3.3}}{\theta_{amb}}$$

The P3T3 method can be written substituting this pressure correction equation:

$$EICO_{alt} = EICO_{sl} \left( \frac{\delta_{amb}^{3.3}}{\theta_{amb}^{1.02}} \right)^x$$

$$EIHC_{alt} = EIHC_{sl} \left( \frac{\delta_{amb}^{3.3}}{\theta_{amb}^{1.02}} \right)^x$$

$$EINO_{x,alt} = EIXO_{x,sl} \left( \frac{\theta_{amb}^{1.02}}{\delta_{amb}^{3.3}} \right)^y e^H$$

The values of  $x$ ,  $y$  are the same of the  $P3T3$  method, for each engine. The default values of  $x$  and  $y$  should be used: 1.0 and 0.5 respectively.

Now can write an energy balance across the combustor:

$$\eta_b W_F LHV = (W_F + W_a) C_p (T_4 - T_3)$$

The  $W_F$  is typically less than 2% of the airflow rate, the assumption that the fuel and air are both at the same temperature,  $T_3$ , and that they have the same specific heats can be made, and any small inaccuracies ignored. Equation can then be approximated as

$$\eta_b W_F LHV = W_a C_p (T_4 - T_3)$$

As for  $P3T3$ , assuming the same  $T_3$  and  $T_4$  at sea level and at altitude:

$$W_{F,sl} = W_{F,alt} \frac{W_{a,sl} \eta_{b,alt}}{W_{a,alt} \eta_{b,sl}}$$

The airflow rate into the combustor at sea level is

$$W_{a,sl} = k \frac{P_{3,sl}}{\sqrt{T_{3,sl}}} f(M_3)_{sl}$$

Where  $k = \frac{\sqrt{\gamma}}{\sqrt{RT_3}}$  and  $f(M_3) = M \left( \frac{1}{1 + \frac{\gamma-1}{2} M^2} \right)^{\frac{\gamma+1}{2(\gamma-1)}}$  And the same expression can be translated at altitude:

$$W_{a,alt} = k \frac{P_{3,alt}}{\sqrt{T_{3,alt}}} f(M_3)_{alt}$$

If the combustor exit is choked and the total temperatures at the combustor inlet and exit are assumed to be the same at the sea level and altitude conditions:

$$f(M_3)_{sl} = f(M_3)_{alt}$$

Finally it can be written (with  $T_{3,alt} = T_{3,sl}$ ):

$$W_{F,sl} = W_{F,alt} \frac{P_{3,sl}}{P_{3,alt}} \frac{\eta_{b,alt}}{\eta_{b,sl}}$$

Moreover, the burner efficiency can be related to the fuel air ratio from equation  $\eta_b = \frac{k}{\frac{W_F}{W_a}}$

With:  $k = C_p(T_4 - T_5)/LHV$

The final function for the fuel flow is:

$$W_{F,sl} = W_{F,alt} \frac{P_{3,sl}}{P_{3,alt}} \frac{\frac{W_F}{W_a}_{sl}}{\frac{W_F}{W_a}_{alt}}$$

Substituting previous equation and assuming  $\gamma=1.4$

$$\frac{P_{3,sl}}{P_{3,alt}} = \frac{\theta_{amb}^{3.3}}{\delta_{amb}}$$

Using the standard non-dimensional analysis parameters a relationship between fuel air ratio and combustor inlet temperature can be found:

$$T_{3,sl} = \frac{T_{3,alt}}{\theta_1}$$

And

$$\left(\frac{W_F}{W_a}\right)_{sl} = \frac{\left(\frac{W_F}{W_a}\right)_{alt}}{\theta_1}$$

Plotting “corrected” fuel air ratio with corrected T3, the data can be fitted with a power function:

$$\frac{\left(\frac{W_F}{W_a}\right)_{alt}}{\theta_1} = k \left(\frac{T_{3,alt}}{\theta_1}\right)^X$$

Equation can also be written at sea level, substituting this function in  $W_F$  is obtained:

$$\frac{W_F}{W_a}_{sl} = k(T_{3,sl})^X$$

$$W_{F,sl} = W_{F,alt} \frac{\theta_{amb}^{3.3}}{\delta_{amb}} \theta_1^{X-1}$$

It can be assumed a square relationship ( $x=2$ ) and the equation becomes:

$$W_{F,sl} = W_{F,alt} \frac{\theta_{amb}^{3.3}}{\delta_{amb}} \theta_1$$

Using the functions for the compressible flow for total to static temperature and pressure:

$$\theta_1 = \theta_{amb} \left( 1 + \frac{\gamma - 1}{2} M^2 \right)$$

$$W_{F,sl} = W_{F,alt} \frac{\theta_{amb}^{3.3}}{\delta_{amb}} \theta_{amb} (1 + 0.2M^2)$$

From perturbation theory  $e^{0.2M^2} = (1 + 0.2M^2)$   
Equation may be rewritten as:

$$W_{F,sl} = W_{F,alt} \frac{\theta_{amb}^{4.3}}{\delta_{amb}} \theta_{amb} e^{0.2M^2}$$

Choosing an exponent  $z=3.8$  to best collapse the data resulted in the following equation:

$$W_{F,sl} = W_{F,alt} \frac{\theta_{amb}^{3.8}}{\delta_{amb}} e^{0.2M^2}$$

### Installation correction

The emissions are measured bleed off, no horsepower extraction, but most airplane operations are nominal bleed on and nominal horsepower extraction. Horsepower extraction is generally very low during cruise operations, so its impact on fuel flow and  $T_3$  is sufficiently small that it is not taken into account for the *FFM2*. However the emissions indexes relationship with fuel flow and  $T_3$  show a large difference when bleed is on. To account for this a small correction was developed that is applied to each of the ICAO data point fuel flow values. As such there is no logical way to predict when and how they are in use, without airplane cockpit data or onboard monitoring system output. [26]

The size of the factor for each LTO operational mode is shown in the following table:

LTO Mode	Fuel Flow Method
Takeoff	1.010
Climb	1.013
Approach	1.020
Idle/Taxi	1.100

Table 4.3. Correction coefficients

### Curve fitting

The engine manufacturers test for emissions from minimum (idle) to maximum (take-off) power corresponding to the highest rating available for that engine family. However, this data is proprietary to the engine manufacturer and only a subset of it is made public. These data points are those reported to the ICAO Emission Databank. Engine fuel flow,

$EINO_x$ ,  $EIHC$  and  $EICO$  are reported at power settings of idle/Taxi (7%), Approach (30%), Climb(85%) and Takeoff (100%). [26]

Examining database and the literature, it is apparent that the  $HC$  and  $CO$  curves could follow a logarithmic trend at low power while  $NO_x$  is generally linear, but may exhibit some logarithmic trend at higher power. To simplify, and to use a simple common method to fit the data, it was decided to try the logarithmic fit for  $HC$ ,  $CO$  and  $NO_x$ .

### 4.2.1 Methodology

The first step is the curve fitting of the data. The emission indexes ( $NO_x$ ,  $HC$ ,  $CO$ ), from ICAO Databank, are to be plotted (logarithmic curve) with the corrected fuel flow.

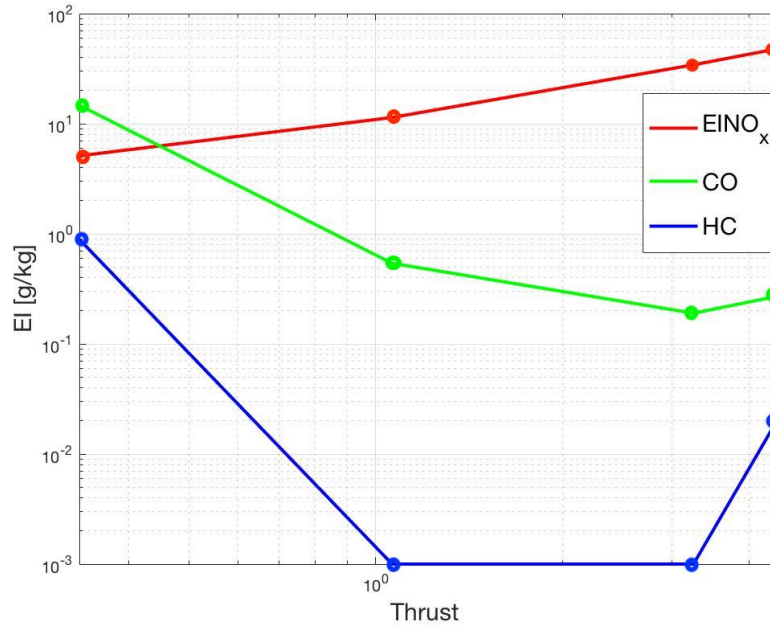


Figure 4.2. Example of a possible curve fitting ICAO Databank

Then, it is necessary to calculate  $\delta_{amb}$  e  $\theta_{amb}$ .

$$\delta_{amb} = \frac{P_{amb}}{14.696}$$

$$\delta_{amb} = \frac{T_{amb} + 273.15}{288.15}$$

where  $P_{amb}$  e  $T_{amb}$  are respectively ambient pressure and temperature. Now it is possible calculate the fuel flow value:

$$W_{F,sl} = W_{F,alt} \frac{\theta_{amb}^{3.8}}{\delta_{amb}} e^{0.2M^2}$$

The humidity correction factor is  $H = -19.0(\omega - 0.0063)$ , where  $\omega$  is the specific humidity,  $\omega = \frac{0.62198\Phi P_v}{P_{amb} - \Phi P_v}$ .  $\Phi$  is relative humidity and  $P_v$  is the saturation vapour pressure [psia].

The final step is to calculate the emission indexes of  $HC$ ,  $CO$  and  $NO_x$ :

$$EICO_{alt} = EICO_{sl} \frac{\delta_{amb}^{3.3}}{\theta_{amb}^{1.02}}$$

$$EIHC_{alt} = EIHC_{sl} \frac{\delta_{amb}^{3.3}}{\theta_{amb}^{1.02}}$$

$$EINO_{x,alt} = EIXO_{x,sl} \left( \frac{\theta_{amb}^{1.02}}{\delta_{amb}^{3.3}} \right)^{0.5} e^H$$

Where the emission indexes at sea level ( $EICO_{sl}$ ,  $EIHC_{sl}$ ,  $EIXO_{x,sl}$ ) are values read off the graph (of the first step) by substituting  $W_{F,sl}$ .

### 4.2.2 Matlab Code

In this first code of Matlab, the program reads and saves the ICAO Databank (file *.xlsx*) in a matrix. After selecting a single engine, the code saves its main characteristics in a vector, as by pass ratio ( $BPR$ ), overall pressure ratio ( $OPR$ ) and the thrust ( $T$ ).

Using a few lines of code, it uses the first two quantities ( $OPR$  and  $BPR$ ) to calculate the pressure and temperature inside the engine in each station (compression, burner, turbine, nozzle). However, it is necessary to enter variables, such as the inlet air flow, number of Mach and the outlet section of the exhaust nozzle.

The thrust can be used to have a comparison with ICAO data, 100% of the thrust (calculated with Matlab code) has to be as similar as possible to that reported on the Excel file, so that the assumptions made are valid.

It is necessary to make a clarification regarding the combustion chamber. In fact, the resulting quantities can be calculated in two different ways:

- keeping the burner outlet temperature fixed (temperature inlet turbine =  $TIT$ )
- keeping the fuel flow rate fixed

For the first case, keeping the  $TIT$  constant, I know the burner inlet air flow rate and therefore, consequently I can obtain  $\alpha = \frac{\eta_b H_i}{c_p (TIT - T_2^0)} - 1$  and  $f = \frac{1}{\alpha}$  and from these values derive the fuel flow rate  $W_f = \dot{m}_0 f$

The second case proceeds in reverse. Knowing  $W_f$  it is possible to calculate  $f$  and subsequently  $T_4^0$ . In this case it is possible to refer to the values of the ICAO database, in fact the code can read and save the fuel flow values for the 4 points of the LTO cycle (takeoff, climb, approach, taxi/idle).

Once the best approach it can be applied for an entire mission. The figure 4.3 is an example carried out with a Trent 892 engine, which performs a mission of about 400 minutes consisting of take-off, climb, cruise, approach and taxi.

This is a typical mission profile for various types of aircraft, it is used for many transport and general aviation designs.

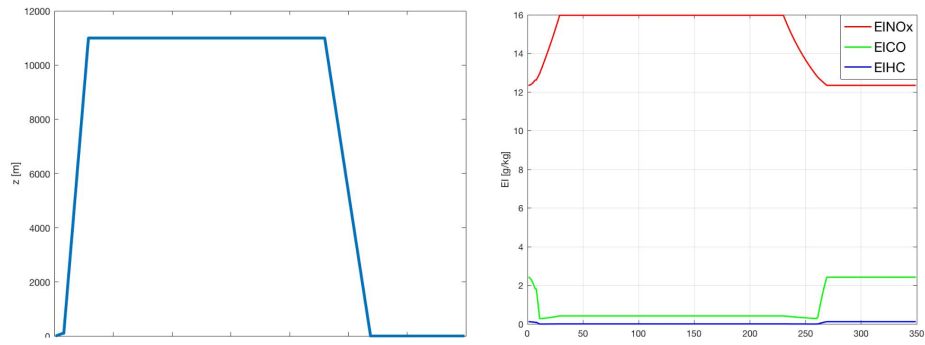


Figure 4.3. Example of a simple mission of a Trent 892

### Emission during an entire mission

By applying the same reasoning for the calculation of emissions during the LTO cycle, it is possible to repropose them in the calculation of the entire mission, to estimate the quantity of combustion products during a typical mission.

In this emissions estimate, the Fuel Flow Method should be used. In fact, the emission indexes at sea level ( $EINO_x$ ,  $EICO$ ,  $EIHC$ ) are obtained from the interpolation of the fuel flow used during the cruise phase. Once the  $EI$  at altitude have been obtained (as reported in the previous section of this chapter), this formula can be used:

$$Emission_{i,k} = EI_{i,k} w_{f,k} \Delta t$$

In figure 4.4, assuming a typical mission, consisting solely of take off, climb, cruise (about 400 minutes), approach and taxi. And thanks to the use of a Matlab code to implement this reasoning, the following results were obtained for a GP7270 engine.

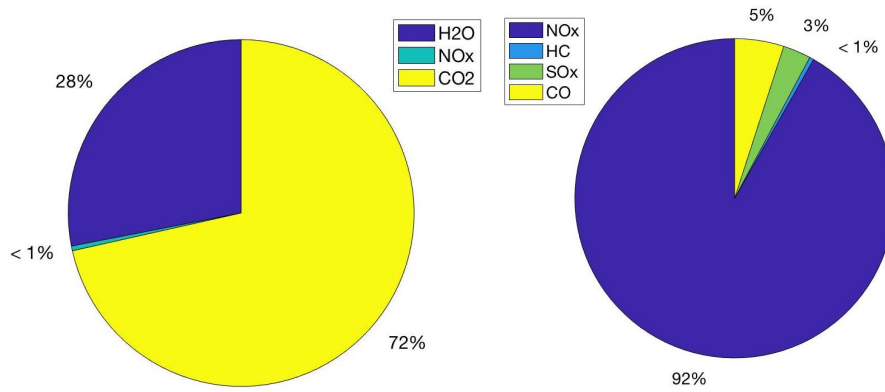


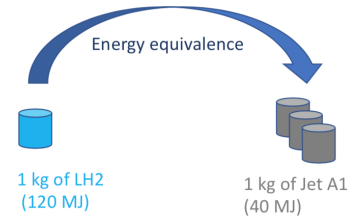
Figure 4.4. Primary and secondary emission during entire mission of GP7270

### 4.3 Fuel Flow Method for $LH_2$ combustion

In this section fits the "Fuel Flow Method 2" in the case of combustion of liquid hydrogen ( $LH_2$ ).

For this reason, the previous code was used to calculate the thermodynamic cycle of the complete engine, in which the calorific value ( $H_i$ ) of Jet A1 is replaced with that of liquid hydrogen. In fact, the  $H_i$  for Jet A1 (typical kerosene used in civil aircraft) is about  $43,3 MJ/kg$ , while, for  $LH_2$  is  $141,1 MJ/kg$ .

If the purpose of the engine is to keep the  $TIT$  constant in order to have an engine with performance similar to the kerosene one, it is intuitive to imagine that the fuel flow decreases as the heat given off by the combustion of hydrogen is significantly greater.



The matlab code confirms this initial hypothesis, and developing the fuel flow method again in this case it will be noticed how, by decreasing the fuel, the number of  $EINO_x$  emissions decreases. Obviously, since the combustion is between air and liquid hydrogen there will be not formation of  $EICO$  and  $EIHC$ .

The figure 4.5 is an example; a graph representing the emissions of a subsonic civil aircraft using Jet A1 and  $LH_2$  during the LTO cycle.

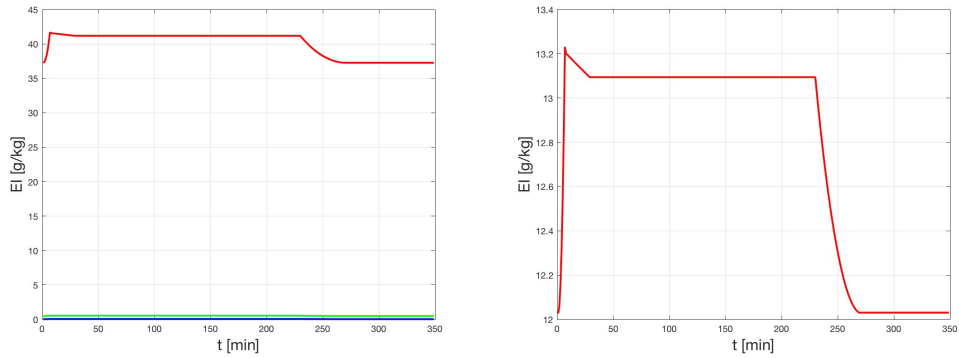


Figure 4.5. Mission with Jet A1 (left) and  $LH_2$  (right)

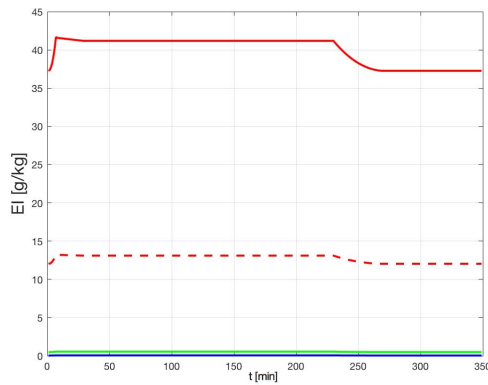


Figure 4.6. Comparison between Jet A1 and  $LH_2$  (dashed)

With the same Matlab code of the previous section it is possible calculate the emission quantity during the mission with  $LH_2$ .

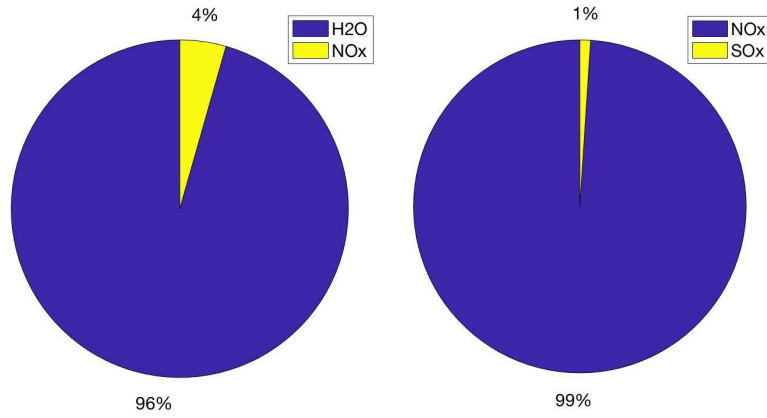


Figure 4.7. Primary and secondary emission during entire mission of GP7270 with  $LH_2$



## Chapter 5

# Hypersonic flight

A problem of fluid dynamics or aerodynamics is said to be in a supersonic regime if the characteristic velocities of the motion field are greater than the speed of sound in the fluid considered with respect to a reference system integral with the body. The behavior of a supersonic flow is very different from that in a subsonic regime. The speed of sound is the maximum speed at which a fluid dynamic disturbance can propagate in a fluid.

Supersonic flight brings with it substantial technical challenges, as the aerodynamics of supersonic flight are dramatically different from those of subsonic flight. In particular, aerodynamic drag rises sharply as the aircraft passes the transonic regime, requiring much greater engine power and more streamlined airframes. To keep drag low, wingspan must be limited, which also reduces the aerodynamic efficiency when flying slowly. Since a supersonic aircraft must take off and land at a relatively slow speed, its aerodynamic design must be a compromise between the requirements for both ends of the speed range.

To maintain a supersonic flight regime, turbojets or alternatively turbofans with a low by-pass ratio can be used with the addition of afterburners. These configurations allow to overcome the transonic regime and fly at speeds greater than Mach 1.

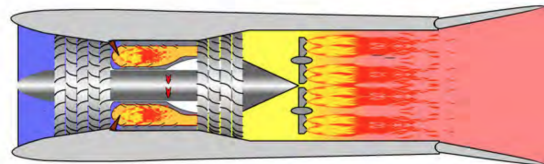


Figure 5.1. Turbojet with afterburner

An alternative is to use ramjet and scramjet. Ramjet and Scramjet are two types of air-breathing engines, classified as exoreactors as they exploit oxygen, naturally present in the air, as an oxidant in the combustion reaction. The substantial difference between the two systems consists in the combustion process: the Scramjet (Supersonic Combustion) in fact provides for a supersonic combustion, as opposed to the “usual” subsonic combustion of the ramjet.

The Ramjet and Scramjet structure can be thought of as a single aerodynamic duct, essentially reduced to an air intake, a combustion chamber and a final nozzle.

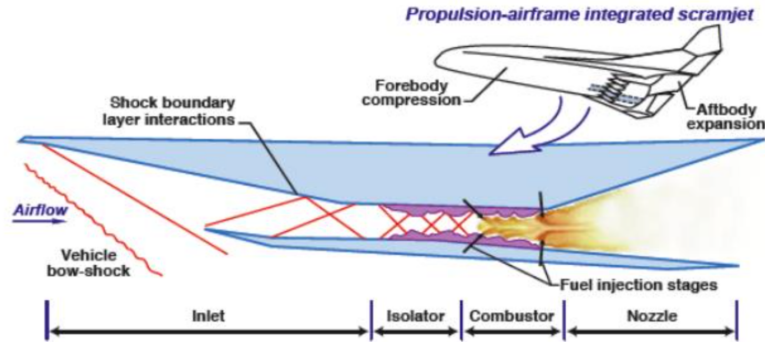


Figure 5.2. Scramjet architecture

In fact both are devoid of rotating parts such as compressors and turbines. In this way it is not possible to establish a relative motion when the aircraft is in stationary conditions, as for example during take off: in fact these systems do not allow take-off. This translates into the need to combine them with turbojet systems, such as the turbofan. This need is also dictated by the fact that both Ramjet and Scramjet achieve high performance in terms of efficiency when they fly in certain optimal conditions: the ramjet flight mach is between 2 and 5, while the one of the scramjet is higher than Mach 5. [25]

A problem of fluid dynamics or aerodynamics is generally considered to be in hypersonic regime for characteristic velocities of the motion field of a Mach number greater than 5. Hypersonic flow phenomena are in particular characterized by viscous interaction phenomena, since viscosity has a strong influence on external flow and shock waves. Shock waves can chemically alter the surrounding air or gas, creating a partially ionized plasma, which reaches a high temperature (aerodynamic heating).

The higher the flight mach, the higher the total input enthalpy is and therefore if the input enthalpy is very high, the fuel provides little energy to the flow and for this it is necessary to change fuel. For this reason, hydrogen is used as a fuel.

The engine is strongly integrated with the aircraft's architecture. There is a very strong coupling between fluid dynamics and architecture.

## 5.1 Ramjet

The ramjet is a jet engine and conceptually the simplest exoreactor. The statorjet reduces the complexity of the simple turbojet by eliminating the compressor and, consequently, the turbine that must drag it, thanks to the speed of the aircraft which compresses the air entering the air intake. As a result, the statorjet is unable to operate at a fixed point (i.e. stationary with respect to air) and has poor performance at low speeds due to the low compression ratio obtained from the air intake. Eliminating compressors and turbines

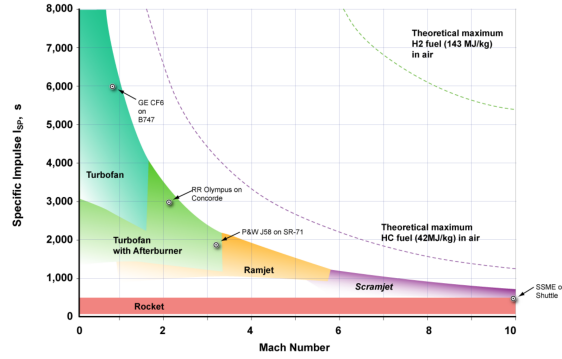


Figure 5.3. Propulsion performance

can be allowed for higher combustion temperatures and consequently higher outflow rates. Raising the total temperature increases the work and increases the thrust. Higher flight speeds can therefore be reached.

The principle of operation of the stator-jet is the same as that of the traditional jet engine. The external air enters a dynamic intake or air intake and is compressed and mixed with the fuel, to then pass into the combustion chamber and then be expelled from the rear through an exhaust nozzle, at a speed higher than the inlet speed. When the air enters this type of jet engine, even if the aircraft is proceeding at supersonic speed, it is slowed down to subsonic speed due to the particular geometry of the ducts, which are shaped to generate a system of oblique impacts. [25]

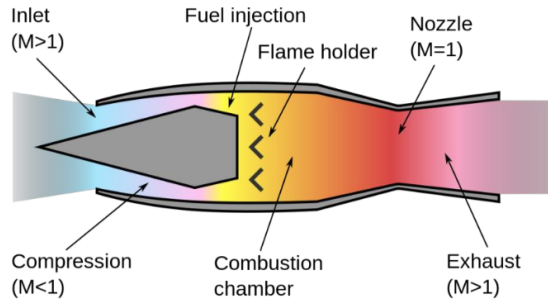


Figure 5.4. Ramjet

The ramjet is purposely built to exploit this compression effect through careful design of the air intake shape. In practice, having no moving parts, this type of motor can be described as a long tube with a variable section.

In the case of an ideal ramjet:

$$T = (\dot{m}_0 + \dot{m}_g)u_9 - m_0u_0 + A_9(p_9 - p_0)$$

$$\frac{T}{\dot{m}_0} = (1 + f)u_9 - u_0$$

This is an engine performance parameter, where  $T$  is the thrust,  $\dot{m}_0$  is the inlet flow, the  $\dot{m}_g$  is the outlet flow,  $u$  instead is the speed of the flow. The project parameters are: flight Mach  $M_0$ , altitude  $z$  and output temperature from the combustor  $T_4^0$ .

$$\begin{aligned}
 u_0 &= M_0 a_0 = \frac{M_0}{\sqrt{\gamma R T_0}} \\
 u_9 &= M_9 a_9 = \frac{M_9}{\sqrt{\gamma R T_9}} \\
 \rightarrow T_9 &= \frac{T_9^0}{1 + \frac{\gamma-1}{2} M_9^2} = \frac{T_4^0}{1 + \frac{\gamma-1}{2} M_9^2} \\
 &\rightarrow T_9^0 = T_4^0
 \end{aligned}$$

Also remembering that  $p_9 = p_0$  then it is immediate to add that  $M_9 = M_0$ . The outlet mach is the same of inlet, but is very important to remember that the thrust is calculated by the  $u_9$ , and not by mach number.

$$\frac{T}{\dot{m}_0} = (1 + f) M_0 \sqrt{\frac{\gamma R T_4^0}{1 + \frac{\gamma-1}{2} M_0^2}} - M_0 \sqrt{\gamma R T_0}$$

In order to find it, an enthalpy balance on the combustor is performed:  $f = \frac{c_p(T_4^0 - T_0^0)}{H_i - c_p(T_4^0 - T_0^0)}$ , also  $f$  is a function of the flight mach.

In reality we will have losses due to the air intake, nozzle and combustion, so the output Mach 9 is no longer equal to the flight Mach, but rather less.

## 5.2 Scramjet

The Scramjet (supersonic combustion ramjet) is a jet engine conceptually derived from the ramjet. Contrary to conventional turbine engines (turbojet and turbofan), and in analogy with the ramjet, the scramjet does not use rotating parts to compress the air, but the kinetic energy of the incoming air flow and the particular geometry of the air intake instead.

Unlike the ramjet, the air flow inside the engine, even if slowed down, always remains at supersonic speeds. This allows the scramjet to operate efficiently at extremely high speeds, with a theoretical limit not yet established, but still higher than Mach 6. [25]

The internal flow is highly dependent on external aerodynamics.

The structure of the engine is extremely simple, and consists of three main parts: a converging duct where the supersonic inlet flow is compressed and slowed; a combustion chamber in which the fuel in gaseous form reacts with atmospheric oxygen producing heat; a diverging exhaust nozzle where the flow, which in all phases has maintained the conditions of supersonic speed, is further accelerated, producing thrust.

On the other hand, for this type of engine, to work and generate thrust, a very high starting speed in flight is required, so it must be brought into supersonic regime by some other type of engine (rocket engine, turbofan).

In the case of the ramjet, the total enthalpy at point 0 is  $10^6$  because the speed  $u_0$  is very high. If  $u_0$  is further increased to the order of  $10^4$ , a total input enthalpy of  $10^8$  would be obtained. The enthalpy provided by a fuel such as jet A is in the order of  $10^6$ , so it is much less relevant than the energy that the air flow already possesses.  $M$  increases and  $h^0$  increases; when  $h^0$  is similar to  $H_i$  it is necessary change fuel. For this reason liquid hydrogen is used.

There is another element: the isolator, which produces oblique shock waves that slow the flow down. It is a passive device, which prevents an inversion of the flow towards the air intake and serves to compensate for the sudden increase in pressure.

The nozzle must be very long and divergent such as to have  $M$  output equal to  $M$  of flight. Since  $M_0$  and  $M_9$  are the same the nozzle must expand a lot, and therefore it has a large expansion ratio.

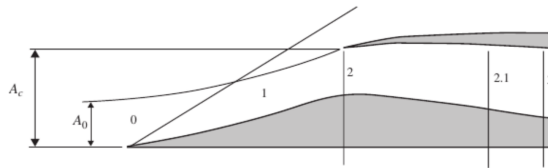


Figure 5.6. Air intake

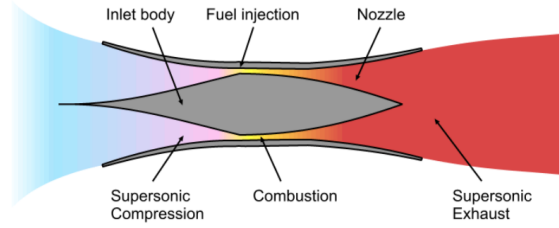


Figure 5.5. Scramjet

The air intake must perform 3 tasks: capturing the right air flow required by the engine, decelerating flow to the right operating condition with the minimum total pressure loss and providing the combustor with a uniform flow (the air flow must not have distortions, the boundary layer distorts the flow, must therefore be aspirated). Obviously it must be of variable geometry.

Since the slowdown was necessary for conventional combustion (in a subsonic flow) to take place, a new combustion model that would be stable in the supersonic regime had to be studied. This would also reduce the total pressure losses which contributed to limiting the operating speed.

Supersonic aerodynamics is characterized by sharp edges to achieve oblique impacts and have a low pressure jump. In the case of hypersonic aerodynamics these shapes cannot be used, as would get too high temperature on the body. The typical forms of hypersonic aerodynamics serve to generate a straight collision: shock wave curved and detached. As  $T^0$  increases and the air dissociates, in supersonic case energy losses would be too high. By increasing the temperature, the external electrons begin to be torn, from  $NO$  begin to form  $O_2$ ,  $N_2$ ,  $O$ ,  $N$ ,  $NO^+$ ,  $O^+$  and  $N^+$ , and continuing to increase the temperature they begin to tear more internal ions, creating  $N^{++}$  and  $O^{++}$  (plasma). If the air were inert, it would be impossible to re-enter from space because a  $T^0$  greater than  $10000K$  would be obtained for several minutes. Dissociating, after the shock wave, the air is made up of  $O_2$  and  $N_2$  at  $10000K$  (*frozen* situation) and at this point, zones of dissociation (*non – equilibrium*) are created. Dissociating heat is removed from the air and therefore

the total temperature decreases and a  $T$  of  $2000K$  reaches the heat shield.

### 5.3 Air Turbo Ramjet (ATR)

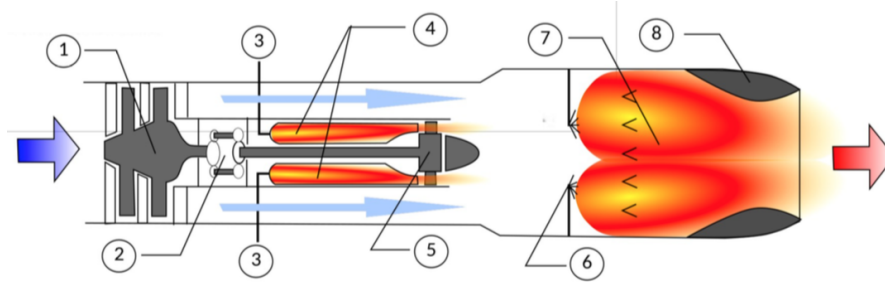


Figure 5.7. Air Turbo Ramjet

For these two types of supersonic engine it is necessary to exploit a particular method of acceleration to be able to operate them: the *Air Turbo Ramjet*. The mission of the air turbo-rocket engine is to accelerate from takeoff to Mach 4.5, where a dual-mode ramjet (DMR) accelerates further to cruise speed.

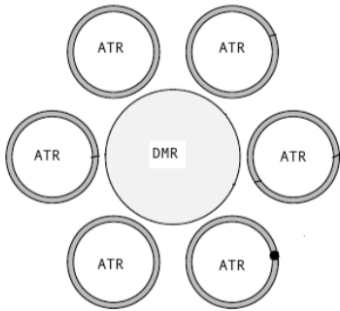


Figure 5.8. Dual Mode Ramjet

In the figure 5.7 is possible to highlight the fan (1), that compresses air from intake, the gear box (2), the hydrogen lines and the turbine (3-4). A mixer is used to blend the air-flow with the primary flow. If the aircraft goes in supersonic field, the ramjet burner fuel injector and main combustor are activated (6-7), and the exhausted gas is ejected from nozzle (8).

A Dual Mode Ramjet (DMR) is a ramjet engine which can be operated in both subsonic and supersonic combustion mode. DMR operation can be obtained by using a fixed geometry if the overall Mach number range is not too wide (i.e. Mach 4 to 8). Extension of this Mach number range, and particularly towards lower Mach numbers, implies variable geometry for the air inlet and/or the combustion chamber.

Nevertheless, different solution can be envisaged in order to obtain satisfactory operation of a DMR in the range Mach 2 to 12 within a single integrated engine.

As a very large flight Mach number range must be considered for the dual-mode ramjet (i.e. 1.5 to 12), a variable geometry is necessary to provide the best acceleration capability

of the air breathing mode.

The analytical study which follows aims to identify the set of meaningful variables that characterize the performance of the air turbo-rocket expander cycle. In order to simplify the formulation, nevertheless without losing generality, the air and the gaseous hydrogen are supposed to be perfect gases, the subcooled hydrogen through the fuel pump is considered an incompressible liquid with constant specific heat capacity ( $C_h$ ) and the intake is assumed ideal ( $TPR = 1$ ). Hence, the specific work across the fan, pump and turbine is respectively:

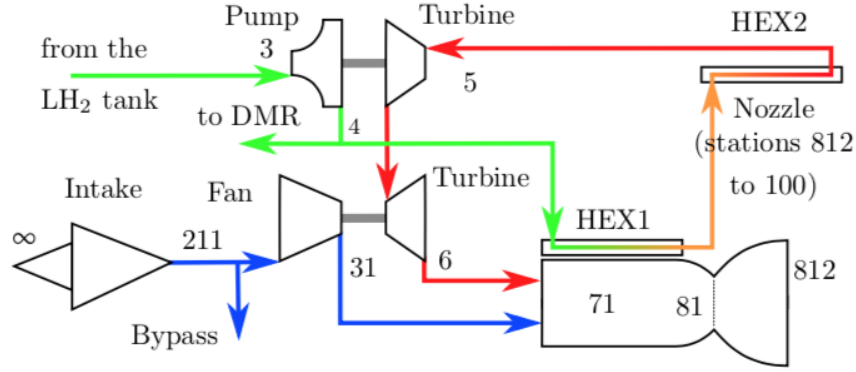


Figure 5.9. Air Turbo Rocket cycle

$$\Delta H_f = \frac{T_\infty^0 C_{p,a}}{\eta_f} (\pi_f^{\frac{\gamma_a-1}{\gamma_a}} - 1)$$

$$\Delta H_p = \frac{(\pi_p - 1) p_3^0}{\eta_p \rho_3^0}$$

$$\Delta H_t = T_5^0 C_{p,h} \eta_t \left( \left( \frac{1}{h_t} \right)^{\frac{\gamma_h-1}{\gamma_h}} \right)$$

The subscripts  $a$  and  $h$  represent the properties of air and hydrogen, and  $f$ ,  $p$  and  $t$  refer respectively to the performances of the fan, pump and turbine. The turbine expansion ratio is expressed as function of the pressure loss across the heat exchanger ( $p$ ), the pump and fan pressure ratios and the ratio of ambient to fuel tank pressures as:

$$\pi_f = (1 - \delta_p) \frac{\pi_p}{\pi_f} \frac{p_3^0}{p_\infty^0}$$

$$\delta_p = \frac{p_4^0 - p_5^0}{p_4^0}$$

the turbine inlet total temperature is calculated by

$$T_5^0 = T_3^0 + \left(\frac{1}{\eta_p} - 1\right)(\pi_p - 1) \frac{p_3^0}{C_h \rho_3^0} + \frac{q}{C_{ph}} MR$$

where the second term on the right hand side is the temperature rise across the pump, and the third term is the temperature increase throughout the heat exchanger by a heat addition of  $q$  per unit of air mass flow. The mixture ratio is referred to the flows through the combustion chamber:

$$MR = \frac{\dot{m}_{31}}{\dot{m}_3}$$

An energy balance applied to the turbomachinery yields that the power required by the fan and the pump equals the power delivered by the turbine:

$$MR\Delta H_f + \Delta H_p = \Delta H_f$$

The cycle performance ( $Y$ ), is uniquely determined as function of 4 variables, namely the fan pressure ratio, the mixture ratio, the heat pick-up and pressure loss across the heat exchanger:

$$Y = f(\pi_f, MR, \frac{q}{C_{ph}T_3^0}, \delta_p)$$

The energy is conserved within the control surface which surrounds the engine:

$$H_3 + MRH_\infty = (MR + 1)H_{81}$$

the throat enthalpy is solely function of the mixture ratio:  $H_{81}$  ( $MR$ ); the flight regime determined by the free-stream stagnation enthalpy. As a consequence, thrust, specific thrust and specific impulse are independent from the chamber thermal load ( $q$ ) and the regenerator pressure drop ( $p$ ); the thrust performances are function of exclusively the chamber pressure, i.e. the fan pressure ratio, the mixture ratio and the flight regime. The calculated specific performances throughout the design space, namely specific thrust, specific impulse and turbomachinery specific work, are considered independent of the engine size, i.e. nozzle throat area. In this manner, the engine can be rescaled to fulfill the mission requirements.

### 5.3.1 LACE

The *Liquid Air Cycle Engine* (*LACE*) exploits the cooling capacity of the cryogenic hydrogen to produce liquid air from the atmosphere. The liquid air (*LAIR*) is then injected with the gaseous hydrogen into a rocket engine to produce thrust.

Precooled engines, in the form of LACE, were first proposed in the 1960's as a propulsion concept for use in the United State's "Aerospaceplane" project.

The cooling capacity of the cryogenic hydrogen is used to produce liquid air (LAIR) from the atmosphere so that it can be mechanically compressed easily and injected together with the now gaseous hydrogen into a rocket engine, where they chemically react to provide thrust. This is a direct way of obtaining oxygen for combustion from the surrounding

atmosphere rather than carrying it onboard.

The key parameter of LACE performance is the ratio of the mass of air liquefied per unit mass of hydrogen expended, a quantity referred to as the Condensation Ratio (CR). The condensation ratio is, in fact, the inverse of the fuel/air ratio  $f$ , that is

$$CR = \frac{\dot{m}_0}{\dot{m}_f} = \frac{1}{f}$$

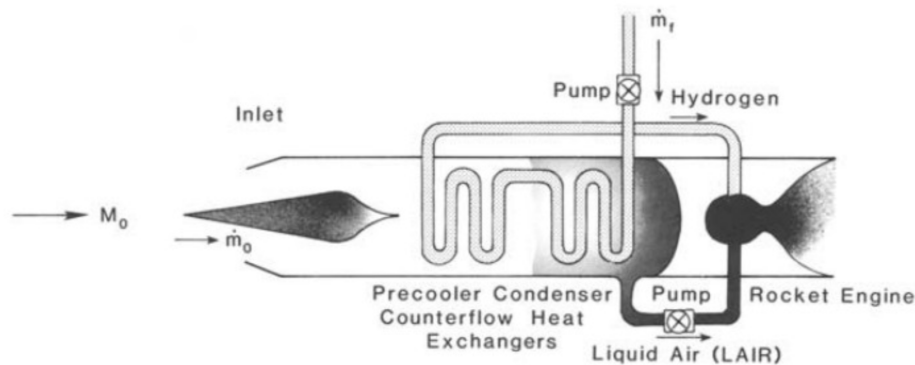


Figure 5.10. LACE

### 5.3.2 SABRE

*Synergistic Air – Breathing Rocket Engine (SABRE)* is the evolution of LACE and LACE-like design. The main difference is that the air is pre-cooled but not liquified. After cooling the air is compressed with a very high pressure ratio (about 200). A *He*-cycle is added which exploits air/*LH*<sub>2</sub> temperature differences to produce power. The power is used to drive air and *He* compressors. The compressed air is used in a combustion chamber, and during off-design operation possible air excess is burned in auxiliary ramjets.

In the figure 5.11 on the following page is possible to see the air cooling down by *He*. It is then compressed at lower temperatures and sent to the main combustion chamber (rocket). Some air may bypass the pre-cooler and is sent to ramjets.

*He* is used in a closed cycle. Heat  $Q_1$  comes from air pre-cooler (HX1) and, if needed, from preburner gas (HX3). *H*<sub>2</sub> is heated by *He* (HX4). *H*<sub>2</sub> expands in the *LH*<sub>2</sub> turbine and in turbine that drives *He* Circulator. Then *H*<sub>2</sub> is sent to Preburner.

The turbine power loop is designed to operate at constant pressure and temperature ratios at all operating points, the power level being varied by changing the helium content of the loop and hence the system pressure. This in turn changes the power loop mass flow in direct proportion to the pressure and the turbine power is directly proportional to the helium mass flow since the temperature drop in the turbine is constant.

For efficient operation it is essential that these nozzles have the correct throat area to pass the flow under the upstream pressure and temperature conditions, and the correct exit area to expand them efficiently to prevailing ambient conditions.

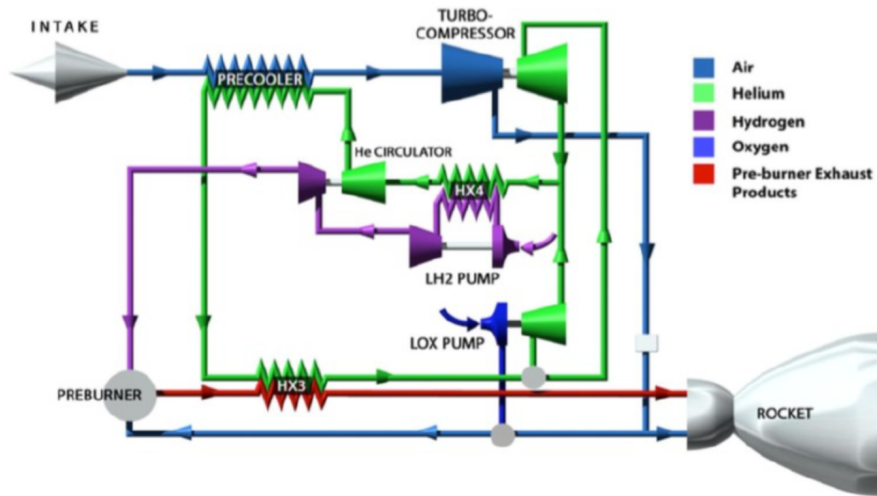


Figure 5.11. SABRE system

In subsonic mode the internal pressure of the jet core may be depressed below ambient, resulting in substantial induced base drag. In supersonic mode the design needs to minimise the shock losses as the two separate flows merge within the same nozzle. The dual flow mode is only present during vehicle acceleration and a practical nozzle which performed slightly less than the ideal would be acceptable. [25]

In cruise modes only one nozzle or the other, i.e. bypass or core engine, is in operation. The mechanical design is complex and will require a substantial study to derive the pressure and thermal loads, structure, cooling and actuation details.

# Chapter 6

## Supersonic emission method

This chapter aims to make changes to the Boeing Fuel Flow Method 2, in order to apply it to the supersonic case.

In fact, if the formulas of the subsonic case are used, as in chapter 4, for the high velocities of the supersonic or hypersonic field, the results cannot be considered valid.

An example of this statement can be seen immediately by observing the exponent of the Mach number in the formula for calculating the fuel flow at sea level. In fact it is equal to two. This implies that for a high Mach number the value of  $W_{f,sl}$  becomes too high and unreliable.

$$W_{F,sl} = W_{F,alt} \frac{\theta_{amb}^{3.3}}{\delta_{amb}} \theta_{amb} (1 + 0.2M^2)$$

### 6.1 Modifications to the subsonic method

The whole derivation of the Fuel Flow Method is then retraced, highlighting the main steps.

The first step is the analysis of the  $X$  and  $Y$  exponents of the combustors. Their values, as previously mentioned, are based on experimental data and are different for each engine. From the various bibliographic sources no method has emerged for calculating them and they are always assumed as values taken from a statistical study. For this reason, even in this thesis work, it is necessary to consider them constant to the previous case, as it is not possible to specify them for ATR, ramjet and scramjet. And so:

$$X = 1$$

$$Y = 0.2 - 0.5$$

After this, the relationship between station number 1 (inlet) and station number 3 (combustor) was modified. In fact, an isentropic relationship is used in the paper, because it still has a good degree of approximation. This relationship can then be modified and a

polytropic or, in the case of ramjet and scramjet, law of compression of the shock waves can be used.

$$\frac{T_3}{T_1} = \left( \frac{P_3}{P_1} \right)^{\frac{\gamma-1}{\gamma\eta_p}}$$

Or with normal shock wave:

$$\frac{P_2}{P_1} = \frac{2\gamma M_1^2 - \gamma + 1}{\gamma + 1}$$

In case a oblique shock wave is considered, is simply needed use a relation between normal velocities and geometry.

After this, there is the assumption that the temperature at station 3 is the same at altitude and at sea level. In the following section, it is assumed that this relationship is not verified and through some supersonic aircraft data it is attempted to interpolate them with a curve and look for a relationship between the temperature difference at sea level and at altitude, with the Mach number.

This data can be confirmed with a quick theoretical reasoning: in fact, with the same number of flight Mach, the thrust of the engine is proportional to the inlet air flow. The inlet air flow is equal to:

$$\dot{m} = \rho u A$$

For this reason, as the altitude increases, the density decreases and therefore:  $\rho_z < \rho_0$ . And so, the thrust at sea level at constant Mach is greater than the thrust at altitude. It is therefore intuitive to think that the temperature of the combustor, at high altitude, is lower than the one at sea level.

$$T_z < T_0$$

$$T_{3,z} < T_{3,sl}$$

Analyzing the Matlab code and the data reported in the paper *STRATOFLY MR3 – how to reduce the environmental impact of high-speed transportation*, it was possible to get to the following statement:

$$T_{3,sl} - T_{3,alt} = 16M^2 + 86$$

Surely this interpolation has given such satisfactory results because it is flawed by the few data available. However, I believe that it can represent how the variation between the temperature at sea level and at altitude is greater and that it cannot be neglected during supersonic flight.

Another delicate step is the consideration of the inlet section of the combustor. Considering that a mobile geometry will be used, it is believed that also for the supersonic case

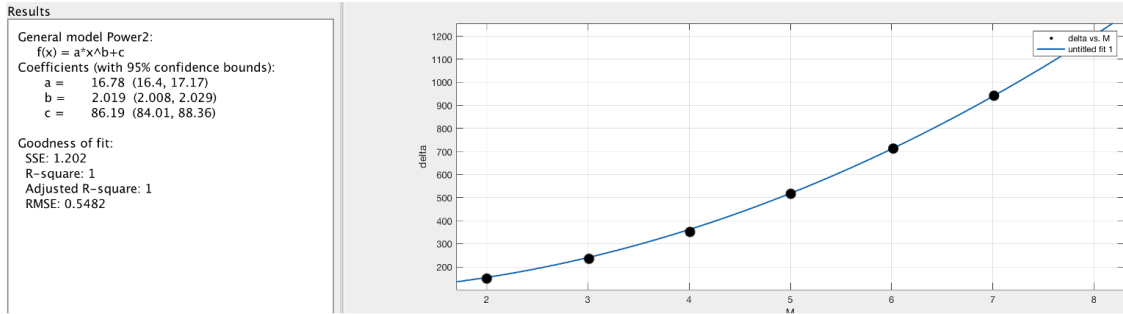


Figure 6.1. Curve fitting  $T_{3,sl} - T_{3,alt}$  and M

it can be considered as checked.

The final step is the study of the relation between Fuel Air Ratio ( $FAR$ ) and  $T_3$ .

In fact, in the paper about the fuel flow method a relationship between these two quantities is obtained through a graphical representation of  $FAR$  and  $T_3$ , from which a second degree curve is obtained. In the case of supersonic flight the same procedue could be carried out, by searching for a new curve that best describes the data provided.

Due to the fact that nowadays there are no sufficient data available for supersonic aircrafts, another method to obtain this curve was needed. In "*Aircraft design: a conceptual approach*" by Raymer there is a relationship between specific consumption and Mach number:

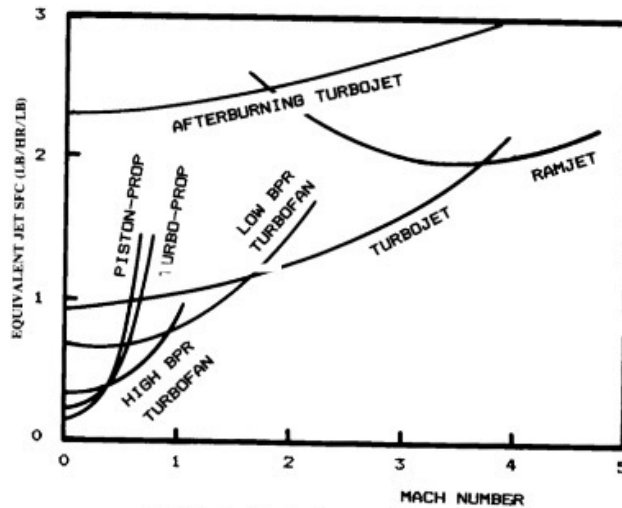


Fig. 3.3 Specific fuel consumption trends.

Figure 6.2. Specific fuel consumption trends

How it can be seen in the previous figure, the turbofan is represented with a second degree curve. A *DMR* is instead similar to a turbojet engine during the take-off and to a ramjet engine in cruise.

Thus, comparing this graph with a possible *FAR-T<sub>3</sub>* graph during the supersonic flight of a *DMR*, it is possible to assume that the function represented is not of second degree, but lower.

The conclusion is that there is a lower dependance on the Mach number in the calculation of the fuel flow with respect to the subsonic case.

And so, the final function is:

$$W_{f,sl} = W_{f,alt} \frac{\theta_{amb}^{\frac{\gamma p}{\gamma-1}}}{\delta_{amb}} \left( \frac{T_{3,sl}}{T_{3,alt}} \right)^{\frac{\gamma-1-\gamma p}{\gamma p} + x} \theta_1^{x-1}$$

$$W_{f,sl} = W_{f,alt} \frac{\theta_{amb}^{\frac{\gamma p}{\gamma-1} + x-1}}{\delta_{amb}} \left( 1 + \frac{\gamma-1}{2} M^2 \right)^{x-1} \frac{T_{3,sl}^{\frac{\gamma-1}{\gamma p} + x-1}}{T_{3,alt}}$$

from which the emission indexes are calculated:

$$EICO_{alt} = EICO_{sl} \left( \frac{P_{3,sl}}{P_{3,alt}} \right)^X \left( \frac{FAR_{sl}}{FAR_{alt}} \right)^Z$$

$$EIHC_{alt} = EIHC_{sl} \left( \frac{P_{3,sl}}{P_{3,alt}} \right)^X \left( \frac{FAR_{sl}}{FAR_{alt}} \right)^Z$$

$$EINOx_{alt} = EINOx_{sl} \left( \frac{P_{3,alt}}{P_{3,sl}} \right)^Y e^H \left( \frac{FAR_{alt}}{FAR_{sl}} \right)^Z$$

The only variable to be determined is therefore the exponent  $x$  for the calculation of the fuel flow. For a more precise analysis it would be advisable to determine exactly the value of the exponents  $X$ ,  $Y$  and  $Z$ , typical of each type of combustor.

## Chapter 7

# Application of supersonic emission method

In this chapter, the considerations from the previous one are applied to Stratofly. Through the data of the numerical simulations carried out by the Von Karman Institute, a Matlab code was developed that would allow to follow the same method of the subsonic flight.

Then the calculations are carried out starting from the following expression:

$$W_{f,sl} = W_{f,alt} \frac{\theta_{amb}^{\frac{\gamma_p}{\gamma-1}+x-1}}{\delta_{amb}} \left(1 + \frac{\gamma-1}{2} M^2\right)^{x-1} \frac{T_{3,sl}^{\frac{\gamma-1}{\gamma_p}+x-1}}{T_{3,alt}}$$

The available data are the flight Mach  $M$ , the flight altitude  $z$ , the fuel flow used during these flight phases  $W_{f,alt}$  and the combustor temperature  $T_{3,alt}$ . Through the numerical code that simulates Stratofly, it was also possible to obtain the relationship between the temperature of the combustor at sea level and at altitude, as a function of the flight mach.

The calculations were then carried out for 5 supersonic flight phases, in which all the parameters were known, and the results are the following:

$M$	$z$ [m]	$W_{f,alt}$ [kg/s]	$W_{f,sl}$ [kg/s] "new" formula	$W_{f,sl}$ [kg/s] classic formula
1.5	14134	448.98	1208.7	1080.7
2	15911	537.23	1546.2	1463.0
3	18975	495.48	1783.7	1538.4
4	22852	242.19	3063.7	2797.6
4.5	23110	366.36	1945.4	1671.0

Table 7.1. Different results during calculation of  $W_{f,sl}$  with adaptation of FFM2

It is noticed that the results compared to the subsonic fuel flow formula are not very

different. In fact, although the values diverge, as the Mach number increases, the temperature ratio stays very close to 1 and therefore the formulas are very similar.

To carry out the calculations, the values of the exponents were kept equal to those of the subsonic flight because there wasn't possibility to obtain new ones. In fact these values are deduced from a study of the different types of combustors and from the following statistical analysis.

It is important to recall that, referring to the figure shown in Raymer's "Aircraft design: a conceptual approach", a quadratic relationship was maintained between the Fuel Air Ratio and the temperature in the combustor.

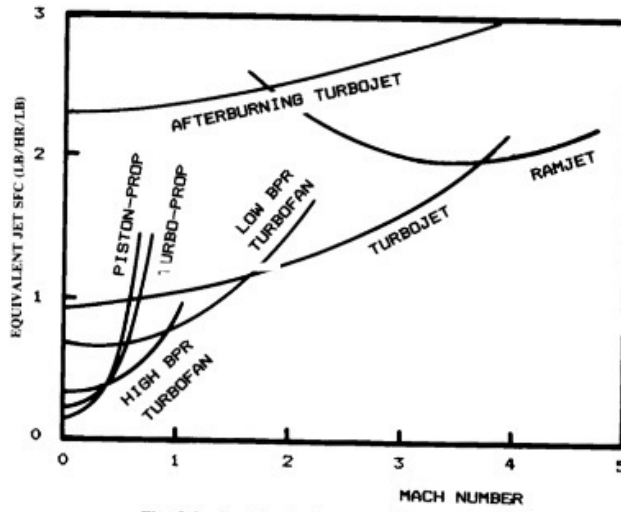


Fig. 3.3 Specific fuel consumption trends.

Figure 7.1. Specific fuel consumption trends

In fact, as it can be seen, even for the Ramjet the reference curve is a parabola, but with a different coefficient compared to the turbofan. However, this term is simplified during the calculation and is therefore irrelevant.

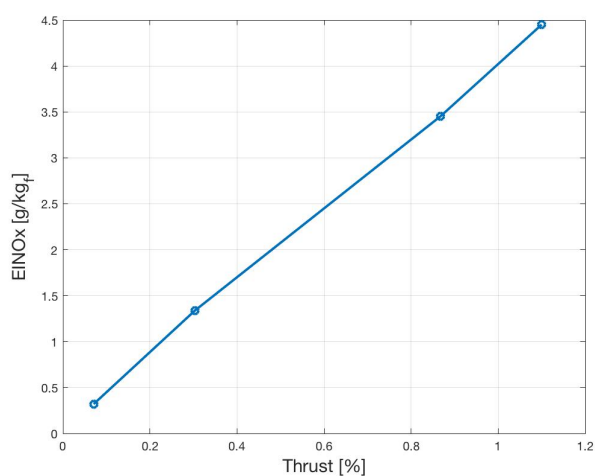
$$\begin{aligned} \frac{\left(\frac{W_f}{W_a}\right)_{alt}}{\theta_1} &= k \left(\frac{T_{3,alt}}{\theta_1}\right)^X \\ \left(\frac{W_f}{W_a}\right)_{sl} &= k T_{3,sl}^X \\ \rightarrow \left(\frac{W_f}{W_a}\right)_{sl} &= \left(\frac{W_f}{W_a}\right)_{alt} \theta_1^{x-1} \end{aligned}$$

At this point some reference values have been selected for the 4 phases of the LTO cycle: both for the fuel flow  $W_f$  and for the Emission Index  $EINO_x$ .

<i>LTO</i>	$EINO_x$ [ $g/kg_{fuel}$ ]	$W_{f,alt}$ [ $kg/s$ ]
100% T	4.45	850
85% T	3.55	537
30% T	1.34	285
7% T	0.32	60

Table 7.2. Characteristic points of LTO cycle

Then the same steps as the ones for subsonic flight were carried out and therefore the interpolation graph was obtained:



As it can be immediately noticed from the next table the values obtained from supersonic emission method aren't very different from the Fuel Flow Method in subsonic case ones:

$EINO_{x,sl}$ [ $g/kg_{fuel}$ ] supersonic method	$EINO_{x,sl}$ [ $g/kg_{fuel}$ ] subsonic method
5.44	5.39
6.43	6.37
7.91	7.81
6.90	6.78
10.87	10.67

Table 7.3. Emission Index at sea level with FFM2 and adaptation at supersonic field

From the data obtained from the Stratofly simulations, the Emission Indexes produced by the aircraft in certain flight conditions are already known. It can therefore be verified whether the data obtained through the emission method in the supersonic field are comparable to the experimental data.

$M$	$z$ [km]	$W_{f,alt}$ [kg/s]	$EINO_{x,alt}$ [g/kg $LH_2$ ] experimental data	$EINO_{x,alt}$ [g/kg $LH_2$ ] computed
1.5	14.134	448.98	8.61	3.81
2	15.911	537.23	11.77	4.36
3	18.975	495.48	24.28	4.10
4	22.852	242.19	3.02	2.67
4.5	23.11	366.36	24.12	3.30
8	33.0	80.0	50.0	2.13

Table 7.4. Differences between Emission Index calculated with FFM2 and experimental data

It is immediate to notice how different the data values obtained with precise fluid dynamics simulations and those with the fuel flow method are. This is due to the fact that there are completely different conditions: much higher altitudes, very high flight Mach numbers, and unknown coefficients to be applied to subsonic formulations to adapt them to supersonic combustors.

It should also be specified that there are very particular conditions during these flight phases. In fact, up to  $M = 4$  only the 6 *ATR* engines are active, while, around Mach 4.5, the *DMR* is activated and only in the hypersonic field (for example  $M = 8$ ) the *ATR* engines are switched off and the aircraft flight is due only to the Scramjet mode. These peculiarities are absolutely not considered during the calculations of the fuel flow method and this also leads to a great uncertainty of the results.

There is a further big problem for the calculation of the emission index: in fact, in the subsonic aircraft there are the 4 typical points of the Landing-Take Off cycle which represent 100%, 85%, 30% and 7% of the rated thrust of the motor. As far as supersonic aircraft are concerned, this is not true: the *DMR* obviously express the maximum thrust (100 % T) during the hypersonic cruise phase and therefore when the scramjet is active. It is therefore not possible to apply the same reasoning as in the previous chapters, as during the take off and climb phases only the 6 *ATR* engines are active, while during the approach and taxi phases both types of engines are even turned off. By interpolating the curve in these 4 points it is not possible to obtain the values of the emission index at sea level in other flight conditions, such as that in the supersonic and hypersonic field. Precisely for this reason it is not possible to properly use the classic fuel flow method for supersonic flight, but, as repeated several times during the thesis work, it will be necessary to make changes based on a large experimental database.

## 7.1 Emissions during supersonic mission

For calculating the emission, the same formula of Chapter 4 is applied:

$$Emission_{i,k} = EI_{i,k}w_{f,k}\Delta t$$

The following graphs are obtained during the LTO phases:

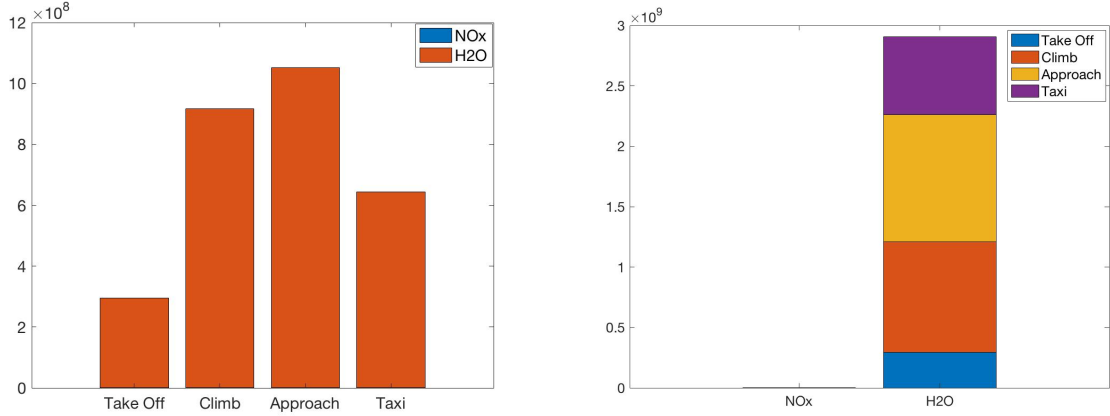


Figure 7.2. Emissions in LTO cycle

Now the same steps can be followed for a full mission. It is important to highlight that Stratofly during Approach and Taxi phases has all the engines off, and so the fuel flow and the emissions are equal to zero. Assuming a classic mission as follows:

Phase	$M$	$z$ [m]	Time [min]	$W_f$ [kg/s]	$EINOx$ [g/kg <sub>f</sub> ]
Take-off	0.3	0	0.7	859.4	4.45
Climb Subsonic	0.4	1'500	2.2	532.6	3.51
Subsonic Cruise	0.5	11'000	25	680	3.57
Supersonic Climb	2	20'000	8	537	6.28
Supersonic Cruise	4	25'000	8	242	37.1
Supersonic Climb	4.5	29'000	8	366	87.5
Hypersonic Cruise	8	33'000	95	80	50
Approach	4	18'000	20	0	0
Taxi/ground idle	0.1	26	26	0	0

Table 7.5. Characteristic points of a typical Stratofly mission

it is possible to carry out the same calculations as in chapter 4 for an entire mission, and it is obtained:

$$NO_x = 1.51 \cdot 10^6 g$$

$$H_2O = 1.43 \cdot 10^9 g$$

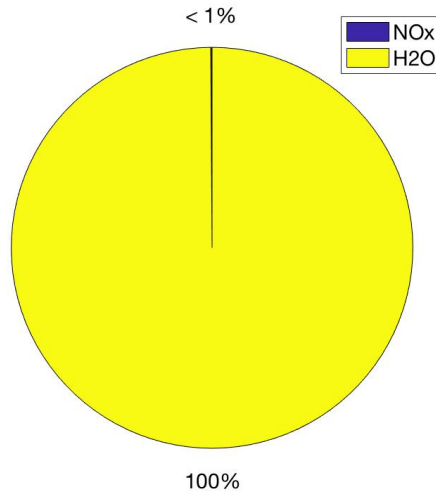


Figure 7.3. Emission during mission

As it can be seen, most of the emissions during a generic mission consist of water vapor.

## 7.2 Comparison between Stratofly and A380

At this point, it is therefore possible to make a comparison between a typical mission of an A380 and a possible one of the DMR Stratofly H2020.

Consequently, the calculations of the previous chapters are carried out on a flight of about 10'000 km (London-Hong Kong), comparing the travel times and emissions of the two types of aircraft:

- A380: 12 hours e 30 minutes
- Stratofly: about 2 hours

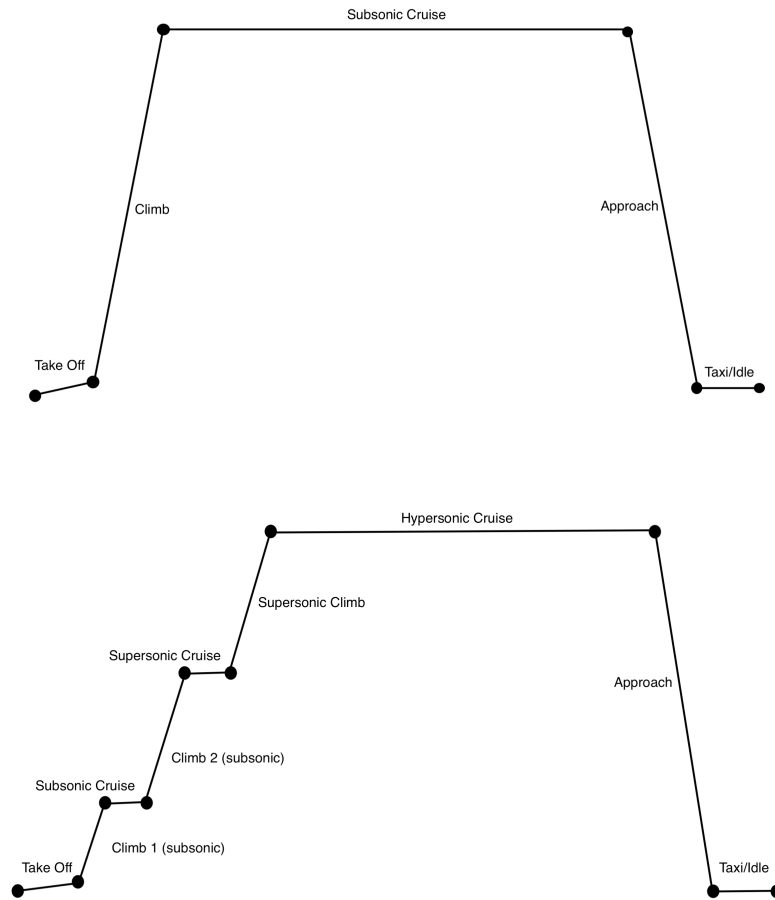
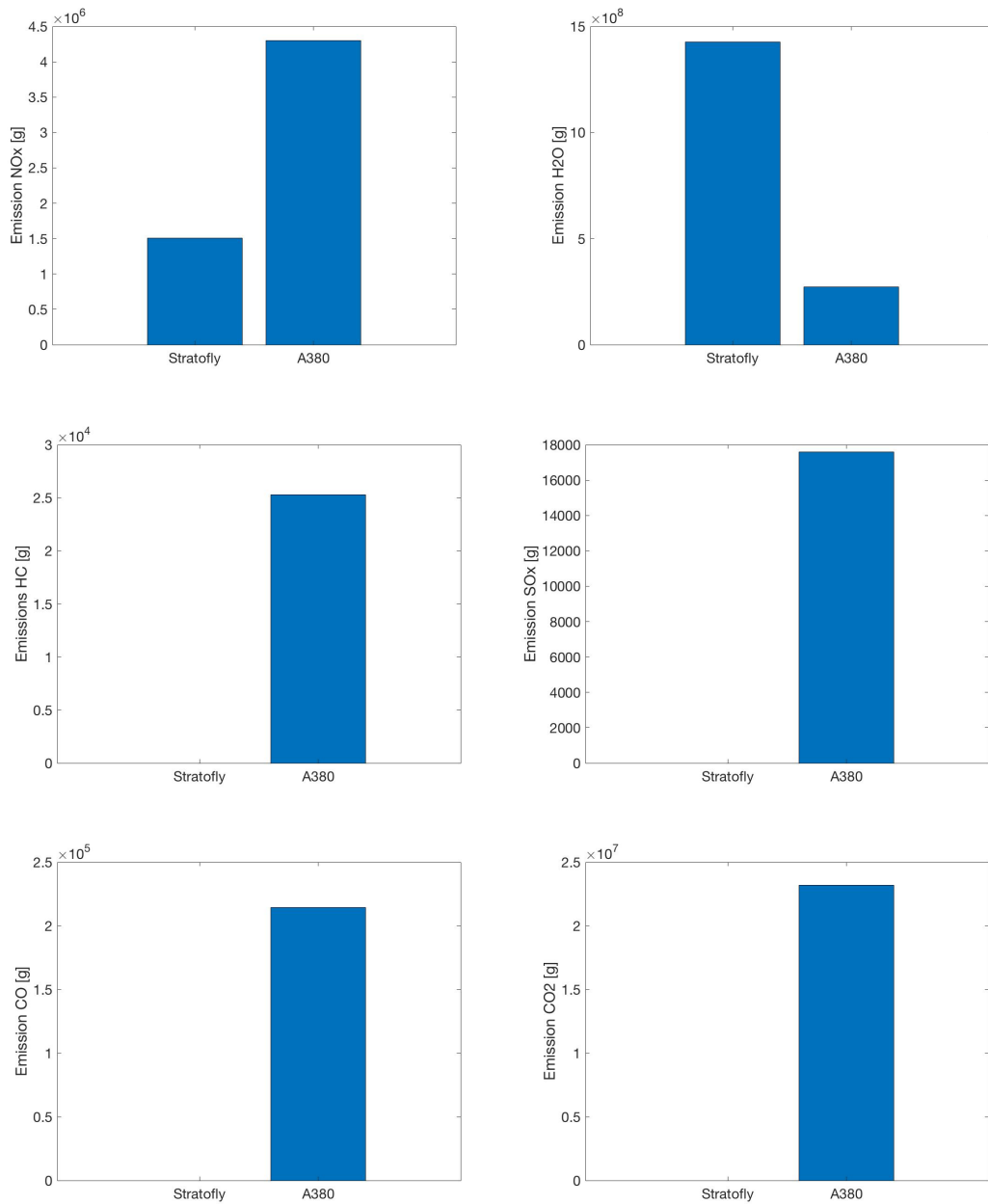


Figure 7.4. Nominal flight mission for A380 and Stratofly

The emissions in a mission of this type are the following:

Emission	Stratofly	A380
$NO_x$	$1.51 \cdot 10^6 g$	$4.30 \cdot 10^6 g$
$H_2O$	$1.43 \cdot 10^9 g$	$2.73 \cdot 10^8 g$
$CO$	0	$2.14 \cdot 10^5 g$
$CO_2$	0	$2.32 \cdot 10^7 g$
$HC$	0	$2.53 \cdot 10^4 g$
$SO_x$	0	$1.76 \cdot 10^4 g$

Table 7.6. Emission during entire mission for Stratofly and A380



Through this analysis it can be seen how convenient it is in terms of emissions to use a ramjet-scramjet engine to perform long distances than the classic subsonic engine.

Obviously this advantage is manifested in the elimination of carbon emissions, which lead to the production of gases that increase global warming. Also, the emissions of  $NO_x$  are much lower than the A380 ones; this data is very important for *Local Air Quality*. In fact, nitrogen oxides are mainly responsible for acid rain and affect the respiratory system

of human beings. Precisely for this reason they must be monitored and kept under control, especially near airports, as *LAQ* could be damaged.



# Chapter 8

## Conclusions

In this thesis work, environmental problems are linked to the air traffic increase. It started by studying the Emission Indexes of aircrafts in circulation at an international level, based on the Icao Database. From this set of data, the first reasonings are developed in order to try to visualize a relationship between the quantity of emissions and the characteristics of the engine. Subsequently, the Boeing Fuel Flow Method was applied, a theory that made it possible to obtain the Emission Indexes of the aircraft along the entire mission profile and not only during the Take off and Landing cycle. Once the Emission Indexes have been obtained it was possible to calculate the quantities of emissions (both during the LTO cycle and during the entire mission) for each type:  $NO_x$ ,  $SO_x$ ,  $H_2O$ ,  $CO$ ,  $CO_2$  and  $HC$ .

After this first part, focused on subsonic flight, was completed, the one, concerning supersonic flight, begins. An attempt was made to adapt the Fuel Flow Method to the supersonic and hypersonic case, retracing the steps taken for subsonic flight. Some simplifications or some steps that would be relevant to high Mach numbers have not been carried out. Subsequently, the formulas with the data obtained by the Von Karman Institute and the "Centro Italiano di Ricerca Aerospaziale" were applied and it was highlighted that the changes made do not particularly differ from the results obtained in the subsonic flight case. Unfortunately, it has not been possible to carry out a statistical analysis for supersonic flight. The available data are not sufficient and there is not a large number of engines used exclusively for supersonic and hypersonic cruises. In fact, ramjets and scramjets are relatively new types of engines and not many examples exist today.

In conclusion, on the one hand for subsonic flight it was not possible to find a relationship between the different types of emissions and the characteristics of each engine ( $OPR$  and  $BPR$ ). On the other hand, it was possible to apply the classic Boeing Fuel Flow Method, which made it possible to obtain the Emission Index during all flight phases. From these values it is immediate to calculate the amount of emissions during an entire typical mission.

In the supersonic and hypersonic field, it was possible to calculate the amount of emissions of a Dual Mode Ramjet engine, through the knowledge of some critical points of

a typical mission. An attempt was made to calculate the Emission Indexes at a precise point of the supersonic mission using the Fuel Flow Method, to see if the data obtained are comparable to the experimental ones. Unfortunately, the data do not match and are very different: this is because coefficients and exponents typical of subsonic combustors are included in the formulas of the fuel flow method and for this reason they must be modified. Furthermore, it must not be forgotten that during the Stratofly mission the DMR is switched on and the six ATR engines are switched off. This important feature will have to be considered in future formulas too, in order to calculate the Emission Index during the typical mission (without knowing the manufacturer's proprietary data).

In the future, having a database of supersonic and hypersonic engines available, it would be interesting to develop a statistical analysis, in order to characterize the emissions of these engines according to their reference parameters. A database would allow to compute new exponents and coefficients for the fuel flow method in the supersonic case, refining and improving the formulas for calculating the Emission Index.

# Bibliography

- [1] Seeckt K., *Conceptual Design and Investigation of Hydrogen-Fueled Regional*, Stockholm, 2010
- [2] *Hydrogen-powered aviation*, Luxembourg, 2020
- [3] Corchero G. and Montanes J. L. *An approach to the use of hydrogen for commercial aircraft engines*, Madrid, 2005
- [4] Nout van Zon *Liquid Hydrogen Powered Commercial Aircraft*, Delft, 2008
- [5] Lentini D., *Impatto ambientale dei motori aeronautici*, Roma, 2018
- [6] Ingenito A., *Modellistica della combustione in regime supersonico*, Roma, 2005
- [7] International Civil Aviation Organization, *Aviation and Environmental Report*, 2019
- [8] International Civil Aviation Organization , *Annex 16-Environmental Protection Volume I, Aircraft Noise*, 2017
- [9] International Civil Aviation Organization , *Annex 16-Environmental Protection Volume II, Aircraft engine emissions*, 2017
- [10] International Civil Aviation Organization , *Annex 16-Environmental Technical Manual, Volume III, Procedures for the CO<sub>2</sub> emission certification* , 2018
- [11] Raymer P. Daniel, *Aircraft design: a conceptual approach*, Washington, 1992
- [12] Fernandez Villacè V., *Simulation, design and analysis of air-breathing Combined-cycle engines for high speed propulsion*, Madrid, 2013
- [13] Longo J. M. A., Dittrich R., Banuti D., Sippel M., Klevanski J., Atanassov U., Carrier G., Dubeau P., Salah El Din I., Thepot R., Loubeau A., Coulouvrat F., Jarsla R., Rabia H., Perigo D., Steelant J., *Concept Study for a Mach 6 Transport Aircraft*, Orlando, 2009
- [14] Okai K., Sippel M., *Component Analysis of TBCC Propulsion for a Mach 4.5 Supersonic Cruise Airliner*, Brussels, 2007
- [15] Jivraj F., Varvill R., Bond A., Paniagua G. *The Scimitar Precooled Mach 5 Engine*, Brussels, 2007
- [16] Murray N., Steelant J., *Methodologies involved in the Design of LAPCAT-MR1: a Hypersonic Cruise Passenger Vehicle*, Bremen, 2009
- [17] C.Paridaens C., Verstraete D., Hendrick P., *Performance Assessment of a Pre-Cooled Turbofan for Hypersonic Vehicle Acceleration*, Brussels, 2011
- [18] Amabile S., Cutrone L., Tuccillo R., Battista F., *Analysis of a Low-Emission Combustion Strategy for a High Performance Trans- Atmospheric Aircraft Engine*, Nashville, 2010
- [19] Haidn O. J., Slavinskava N. A., *Reduced Chemical Mechanism for Methane Combustion*, Toulouse, 2007

- [20] Battista F., Cutrone L., Ranuzzi G., Borreca S., *Supersonic Combustion Models Application in Advanced Propulsion Concepts*, Dayton, 2008
- [21] Langener T., Erb S., Steelant J., *Trajectory simulation and optimization of the Lapcat-MR2 hypersonic cruiser concept*, St. Petersburg, 2014
- [22] Fernandez Villace V., Paniagua G., Steelant J., *Installed performance of an Air-Turbo-Rocket Expander Cycle*, Cologne, 2014
- [23] Jivraj F., Varvill R., Bond A., Paniagua G., *The Scimitar Precooled Mach 5 Engine*, Brussels, 2007
- [24] Ferlauto M., *Appunti del corso di Propulsione Aerospaziale Avanzata*, Torino, 2020
- [25] Marsilio R. *Appunti del corso di Propulsione Aerospaziale Avanzata*, Torino, 2020
- [26] DuBois D., Paynter G. C., *"Fuel Flow Method2" for Estimating Aircraft Emissions*, 2006